Highly variable H_2O/Ce ratios in the Hainan mantle plume

Piao-Yi Wang[a], Xiao-Yan Gu[b,*], Takeshi Kuritani[c], Eero Hanski[d], Qun-Ke Xia[b]

[a] School of Earth and Space Sciences, University of Science and Technology of China, Hefei 230026, China

[b] School of Earth Sciences, Zhejiang University, Hangzhou 310027, China

[c] Graduate School of Science, Hokkaido University, 060-0810, Japan

[d] Oulu Mining School, University of Oulu, P. O. Box 3000 90014 Oulu, Finland

[*] Corresponding author: Xiao-Yan Gu (gxy0823@zju.edu.cn)

Abstract

Mantle plume-generated basalts have long been utilized to assess the large-scale heterogeneity of the deep mantle. Their chemical and isotopic enrichment has been thought to result from the incorporation of recycled sediments or oceanic crust in their sources. Variable extents of dehydration or rehydration of recycled materials during subduction can induce different H_2O/Ce ratios in plume-related basalts. The Hainan plume has been regarded as the cause of the massive Cenozoic basaltic volcanism in southeastern Asia. In this study, we measured bulk-rock major and trace element compositions of basalts from a volcano at Heishanling Hill, northern Hainan Island, and made FTIR analyses of water in clinopyroxene phenocrysts to determine magmatic water contents. In addition, we determined Sr-Nd isotope compositions of basalts at Heishanling Hill and other three localities.

Water contents of Cpx phenocrysts vary from 20 to 254 ppm, which were used to calculate the water contents in the corresponding equilibrated melts, yielding values from 0.22 to 2.42 wt.% with an average of 1.07 ± 0.47 wt.%. Considering the effect of magma differentiation on water contents,

the primary melts of Heishanling basalts were estimated to have a range of 0.67-1.40 wt.% for individual Heishanling basalts, with the average of 1.03 ± 0.33 wt.%. The calculated water contents in the mantle source of the Heishanling basalts vary from 279 to 582 ppm, falling in the range of global OIBs.

Combined with the results previously reported, H_2O/Ce ratios of Hainan basalts were estimated to vary from 50 to 425, covering the reported range from EM-type OIBs to NMORBs. The enriched Sr-Nd isotopic compositions of the studied samples resemble those of other Hainan plume-related basalts, and their $^{143}Nd/^{144}Nd$ ratios are well correlated with incompatible trace element ratios (e.g., Th/La, Ba/Nb). Bulk-rock compositions are consistent with a contribution of pyroxenite in the mantle source of the Hainan basalts and mixing modelling suggests coupled contribution of recycled sediment and oceanic crust. H_2O/Ce displays a negative correlation with $^{143}Nd/^{144}Nd$ and a positive correlation with $(Rb/Nb)_n$ and $(Th/La)_n$, meaning that an increasing amount of recycled oceanic crust and sediment in the source increases its H_2O/Ce. The recycled material incorporated in the Hainan plume source may have undergone variable degrees of dehydration or deep rehydration by fluids released from subcrustal hydrous minerals at grater depths during subduction.

Keywords: H_2O/Ce ratio; water content; the Hainan mantle plume; Hainan basalt; recycled materials; clinopyroxene phenocryst

1. Introduction

Water has long been regarded as an important trace component in the Earth's mantle, affecting its physical properties and partial melting behavior. Experimental studies and numerical modeling have demonstrated that within a subducted oceanic slab, several hydrous or nominally anhydrous minerals can transport a large amount of water into the deep Earth (e.g., Bekaert et al., 2020; van Keken et al., 2011). Plate subduction has also been generally thought to play a crucial role in driving mass recycling of the Earth, delivering large fluxes of surficial material into the Earth's interior. It induces large-scale geochemical heterogeneity in the mantle, as manifested by diverse geochemical endmember components in the composition of basalts (Hofmann, 1997; White, 2015). Oceanic slabs, which are composed of sediments, crustal rocks and upper lithospheric mantle, will experience complex mineralogical reactions upon subduction, including variable degrees of dehydration (e.g., van Keken et al., 2011; Walowski et al., 2015). Despite this, many studies have shown that recycled material can carry a significant amount of surficial water into the deep mantle and thus modify its inventory of water (e.g., Bekaert et al., 2020; Dixon et al., 2017; Hirschmann, 2006). Recycled material can ultimately be entrained into upwelling mantle plumes to engender hotspots, markedly expressed as basaltic magmatism of oceanic island basalts (OIBs; Hofmann, 1997; White, 2015) and large igneous provinces (LIPs; Ernst et al., 2005; Richards et al., 1989).

So far, the amount of water that survives devolatilization and is transported to the deep mantle is not well constrained. Water behaves as an incompatible component during mantle melting, with its incompatibility being similar to that of Ce. Consequently, the H_2O/Ce ratios in basalts are thought to closely reflect the ratio in their mantle source (Dixon et al., 2002). Some previous studies have revealed that large amounts of EM-type OIBs or EMORBs (enriched mid-ocean ridge basalts) have high water contents in their sources but lower H_2O/Ce ratios than those of the depleted MORB mantle (DMM) or the primitive mantle (PM; Fig. 1). This observation has been attributed to the almost complete dehydration of oceanic slabs during their subduction before being incorporated into mantle sources of basalts (e.g., Dixon et al., 2002; Kendrick et al., 2014, 2015; Workman et al., 2006). Higher H_2O/Ce ratios than in DMM and PM have also been reported for some other OIBs and EMORBs, which has been explained by relatively low degrees of dehydration (Fig. 1; Cabral et al., 2014; Jackson et al., 2015; Kendrick et al., 2017; Shimizu et al., 2019) or by rehydration of overlying sediments and crustal rocks in slabs by fluids released from subcrustal hydrous minerals at greater depths (Dixon et al., 2017). OIB-like Cenozoic basalts in eastern China, under which the subducted Pacific slab has been found to be stagnated in the mantle transition zone, show high water contents and H_2O/Ce ratios (up to ~600) (Chen et al., 2017; Liu J. et al., 2015a; Xia et al., 2019). As suggested by Liu J. et al. (2015a), high H_2O/Ce ratios could be associated with a less degree of dehydration related to the cold and fast subduction of the west Pacific plate.

The presence of the Hainan mantle plume in southeastern China has been identified by different geophysical observations (e.g., Montelli et al., 2006; Wei and Chen, 2016; Xia et al., 2016; Zhao et al., 2021) and fits well with a recently developed plate motion model (Zhang and Li, 2018). The plume has been thought to play a crucial role in the tectonic evolution of the region surrounding the South China Sea (SCS; for a review, see Yan et al., 2014). The plume is responsible for the genesis of basalts occurring in the Leiqiong area and the Indochina block as well as EMORBs and seamount basalts beneath the SCS (Fig. 2; e.g., Gu et al., 2019; Wang et al., 2013; Yan et al., 2014; Zhang et al., 2018a). The chemical and isotopic compositions of these basalts indicate that the Hainan plume entrained material with a geochemical affinity of the EM II endmember (An et al., 2017; Flower et al., 1992; Hoang et al., 2018; Tu et al., 1992; Yan et al., 2018; Zhang et al., 2018a, b; Zou and Fan, 2010). Several other studies suggest that the FOZO component might also be incorporated in the source of the Hainan plume-related basalts (e.g., Wang et al., 2013; Tian et al., 2020). The enriched component in the source mantle has been proposed to originate from recycled oceanic crustal material (Liu J.Q. et al., 2015; Wang et al., 2013). The region is surrounded by the convergent boundaries of the Pacific (Philippine) and Indo-Australian plates towards the Eurasian plate (Fig. 2). Subducted slabs have sunk to the lower mantle, even to the base of the mantle, as demonstrated by the presence of bodies with higher-than-average seismic wave velocities in the lower mantle beneath this region (Li et al., 2008). Thus, the Hainan basalts would provide a great opportunity to constrain water recycling in the settings where a deep-rooted mantle plume become spatially associated with subduction of multiple oceanic plates.

In this study, we analyzed water contents and chemical compositions of clinopyroxene (Cpx) phenocrysts in basalts collected from the Heishanling Hill in Hainan Island (China). Bulk-rock elemental and Sr-Nd isotopic compositions were also analyzed for these basalts. Based on these results, water contents in the primary melt of the Heishanling basalts and their mantle source were inversely estimated. We also measured Sr-Nd isotopic compositions of basalts from three other localities (Chitucun, Leihuling and Yongxing) in the northern part of Hainan Island, for which the water content data have been reported previously by Gu et al. (2019). From the whole dataset, we observed that H_2O/Ce in Hainan basalts shows a negative correlation with $^{143}Nd/^{144}Nd$. Furthermore, the basalts have a large range in H_2O/Ce, varying from values similar to the ratios in Samoan OIBs (representing the EM II endmember; Fig. 1) to values exceeding those of MORBs (as high as ~450). Our results provide new constrains on the recycling of water through plate subduction and subsequent entrainment into a deep-rooted mantle plume.

2. Geological background and sample description

The southeastern Asian region is situated in the convergence zone of the Eurasian, Philippine

Sea and Indo-Australian plates (Fig. 2). The complex regional tectonics has resulted in the formation of the South China Sea, a large marginal basin, and intense volcanic activity in the Cenozoic. The magmatism before and during the SCS spreading was relatively weak, and massive basaltic eruptive and intrusive rocks were emplaced later than ~16 Ma, after the cessation of the SCS spreading (Yan et al., 2014). They are mainly distributed over the Leiqiong area, the Beibu Gulf, the Indochina block, and within the SCS basin (Fig. 2). Before the geophysical demonstration of the presence of a low-seismic-velocity anomaly extending to the lower mantle beneath Hainan Island, suggesting the existence of the Hainan mantle plume (e.g., Zhao et al., 2021), the Cenozoic basalts were proposed to be partial melts of metasomatized lithospheric mantle (e.g., Tu et al., 1992) or upwelling enriched asthenosphere (e.g., Hoang et al., 1996). Although the role that the plume played in the initial spreading of the SCS ridge still remains controversial (e.g., Yu and Liu, 2020; Yu et al., 2018; Zhang et al., 2018a), the most popular view suggests that the Hainan mantle plume is the main cause to basaltic magmatism after the Mid-Miocene. The plume-induced basalts mainly display a geochemical affinity to EM II (e.g., An et al., 2017; Yan et al., 2018; Zou and Fan, 2010).

The basalts from Heishanling have Pliocene eruption ages of ~4 Ma (Ho et al., 2000). They host large quantities of peridotite xenoliths, suggesting a rapid ascent to the surface. Most of the studied samples display a porphyritic texture and a groundmass with a low degree of crystallization. The phenocrysts are dominated by euhedral or subhedral olivine and Cpx with sizes of 0.1–1 mm. Detailed petrological descriptions for samples from other three localities (Chitucun, Leihuling and Yongxing) are shown in the supplementary materials of Gu et al. (2019).

3. Analytical methods

3.1 Major and trace element compositions of bulk rocks

Fresh interiors of samples from Heishanling were grinded into 200-mesh powders. The powders were heated to 1000 °C for 90 min, after which the loss on ignition (LOI) was measured. Major and trace elements contents were analyzed by X-Ray fluorescence spectrometry and a PerkinElmer inductively coupled plasma mass spectrometer (ICP-MS), respectively, at ALS Chemex (Guangzhou, China) Co., Ltd. For oxides with contents higher than 1 wt.%, the analytical precision was estimated at 1-3% and for other oxides with contents lower than 1 wt.%, the precision was approximately 10%. For most trace elements, the precision is better than 5%.

3.2 Sr-Nd isotopic compositions of bulk rocks

Strontium and neodymium isotopic analyses for samples from all the four localities were conducted using a multi-collector inductively coupled plasma mass spectrometer (MC-ICPMS; Thermo Fisher Scientific Neptune Plus) at Hokkaido University, Japan. The analytical procedures for the chemical separation of Sr and Nd followed the methods of Pin et al. (1994). The normalizing factors used for internal corrections were $^{86}Sr/^{88}Sr = 0.1194$ and $^{146}Nd/^{144}Nd = 0.7219$. Additional corrections were then performed by applying a standard bracketing method using NIST987 and JNdi-1 for Sr and Nd isotopic analyses, respectively, and normalized to $^{87}Sr/^{86}Sr = 0.710240$ for NIST 987 (Makishima and Masuda, 1994) and $^{143}Nd/^{144}Nd = 0.512117$ for JNdi-1. The Sr and Nd isotopic ratios of JB-3 (from the Geological Survey of Japan) measured during this study, reference values, and standard deviations for replicate analyses are provided in Table A1 of Kuritani et al. (2020).

3.3 Major elements compositions of Cpx phenocrysts

The Shimadzu electron probe microanalyzer (EPMA 1720) at the School of Earth Sciences, Zhejiang University (China), was applied to measure major element compositions of Cpx phenocrysts from Heishanling. The operating conditions were set at an accelerating voltage of 15 kV, a beam current of 20 nA and a beam size of 5 μm. The analyzed positions were placed within or close to the spots analyzed for water by a Fourier transform infrared spectrometer (FTIR). A set of natural and synthetic minerals or oxides were used as standards. The final data are shown after correction using a program based on the ZAF procedure. In every thin section, several large Cpx grains were randomly selected to check the intra-grain compositional heterogeneity with profile analyses.

3.4 Water contents in Cpx phenocrysts

Water contents of clinopyroxene phenocrysts from Heishanling were calculated from infrared spectra based on the modified Beer-Lambert law C_{H_2O}=3A/εt, in which C_{H_2O} is the water content (ppm), A is the integrated absorbance (cm^{-1}), ε is the molar absorption coefficient (7.09 $ppm^{-1}cm^{-2}$ for Cpx from Bell et al., 1995), and t is the thickness of the thin section (cm). Unpolarized IR spectra of Cpx phenocrysts were acquired on double-polished thin sections with the thickness of 0.078-0.178 mm at the School of Earth Sciences, Zhejiang University (China), using a Nicolet iS50 FTIR attached to a Continuμm microscope equipped with a liquid-nitrogen-cooled MCT-A detector and a KBr beam splitter. During the analysis, the entire instrument was flushed with continuous dry air flow. Spectra in the wavenumber range of 1000 to 5500 cm^{-1} were collected on the optically clean, inclusion- and crack-free areas in Cpx phenocrysts using square apertures (30×30 to 100×100 μm^2) adjusted with the size and quality of phenocrysts. The analyzed phenocrysts have diameters ranging from tens of micrometers to >1 mm (along the major axis). 128 scans with the resolution of 4 cm^{-1}

were accumulated for each spectrum. The estimated uncertainty of a single unpolarized FTIR analysis is less than 30% (Liu J. et al., 2015b; Xia et al., 2013).

4. Results

4.1 Geochemical characteristics of Heishanling basalts

Major and trace elements compositions of Heishanling basalts are shown in Table S1. Sr-Nd isotopic compositions of Heishanling basalts and basalts from other three localities (Gu et al. 2019) are reported in Table 1. All the samples have LOI values lower than 1 wt.%. Similar to the basalts from Chitucun, the Heishanling basalts fall in the field of sub-alkaline basalts in the total alkali versus SiO_2 diagram (Fig. 3). MgO contents in the Heishanling basalts range from 9.1 to 11.0 wt.%, being higher than those of the Chitucun basalts, whereas the concentrations of incompatible elements, such as TiO_2 and K_2O, are systematically lower in the Heishanling basalts, ranging from 1.6 to 1.9 wt.% for TiO_2 and from 0.8 to 1.1 wt.% for K_2O (Fig. 4). Variations of major element oxides, FeO/MnO and Ni as a function of MgO suggest that the Heishanling basalts have experienced fractional crystallization of olivine, but no or only little Cpx fractionation (Fig. 4).

The Heishanling basalts show OIB-like primitive mantle-normalized trace element patterns (Fig. 5), which are characterized by strong enrichments in large ion lithophile elements (LILE) and light rare earth elements (LREE), no positive Pb anomalies and the absence of negative Nb-Ta anomalies. Europium and Sr display slightly positive anomalies, with Eu/Eu* (=$Eu_N/\sqrt{Sm_N * Gd_N}$; N indicates normalization to chondrite) and Sr/Sr* (=$Sr_n/\sqrt{Pr_n * Nd_n}$; n indicates normalization to the primitive mantle) ranging from 1.04 to 1.09 and from 1.12 to 1.54, respectively. The steep chondrite-normalized REE patterns with $(La/Yb)_N$ of 8.14-12.49 suggest that the Heishanling basalts left residual garnet in their mantle source (Fig. 6; Liu J.Q. et al., 2015; Zou and Fan, 2010).

Strontium and Nd isotopic compositions of the Heishanling basalts and the samples studied by Gu et al. (2019) show little variation and fall in the range reported previously for basalts related to the Hainan mantle plume (Fig. 6). The covariation of Sr and Nd isotopic compositions indicate that the enriched characteristics in the sources of the basalts related to the Hainan mantle plume may be originally linked with the involvement of the EM II component (Fig. 6).

4.2 Chemical compositions and water contents of Cpx phenocrysts

The calculated water contents of Cpx phenocrysts from Heishanling basalts, along with their major element compositions, are reported in Table S2. Fresh and relatively large Cpx grains were found for FTIR measurements in the four out of the six Heishanling basalt samples that were analyzed for their bulk-rock compositions. Mg# (=molar 100×Mg/(Mg+Fe)) in the analyzed Cpx ranges from 76.7 to 82.9 (Table S2). TiO_2, Cr_2O_3 and CaO display a negative relationship with MgO, whereas SiO_2 increases with MgO (Fig. 7). These relationships are suggestive of crystallization of the analyzed Cpx phenocrysts from the same basaltic magma system.

Figure 8 illustrates representative infrared spectra for Cpx grains from Heishanling basalts. They display three dominant groups of structural OH absorption bands at wavenumbers similar to those reported in previous studies (e.g., Gu et al., 2019; Liu J. et al., 2015b; Xia et al., 2013). The phenocrysts in the Heishanling basalts have a larger range of water contents (20-254 ppm) relative to the analyzed phenocrysts from the other three localities (12-179 ppm; Gu et al., 2019). Water correlates positively with TiO_2, and the calculated fraction of tetrahedrally coordinated Al in Cpx, indicating that the Cpx phenocrysts in the Heishanling basalts have preserved their initial water contents.

4.3 Water contents in melts equilibrated with Cpx and the primary melt of Heishanling basalts

Based on the measured water contents in Cpx phenocrysts, water concentrations in melts equilibrated with them can be calculated using the Cpx-melt partition coefficient of water. Values of this coefficient can be assessed from the major element composition of Cpx by the equation established by O'Leary et al. (2010; Equation 10 therein):

$$\ln D_{H_2O}^{Cpx/melt} = -4.2(\pm 0.2) + 6.5(\pm 0.5) X_{Al^{IV}}^{Cpx} - 1.0(\pm 0.2) X_{Ca}^{Cpx} \quad (1)$$

where $X_{Al^{IV}}^{Cpx}$ and X_{Ca}^{Cpx} are the molar fractions of octahedrally coordinated Al and Ca cations, respectively, calculated on the basis of six oxygen atoms per formula unit of Cpx. The water contents in the melts were calculated from the water contents of Cpx phenocrysts by dividing them by $D_{H_2O}^{Cpx/melt}$. The calculated water contents in melts equilibrated with individual Heishanling Cpx phenocrysts show a range from 0.22 to 2.42 wt.% with the average ranging from 0.79 to 1.42 wt.% for individual samples (Table S1). Considering the combined uncertainties in the Cpx water content estimation and the values of the partition coefficient, the total uncertainty in the calculated water content of the melt is not more than 32% (Liu J. et al., 2015b).

As water behaves incompatibly during magma differentiation, the fractional crystallization of olivine/Cpx will increase water contents in magmas. The correlations between contents of different major elements with MgO contents indicate that the studied Hainan basalts have mainly experienced the fractional fractionation of olivine rather than Cpx (Figs. 4a-h). Thus, we proposed that the fractional crystallization of olivine is the reason for the deviation of bulk rocks from the compositions of their corresponding primary melts. To obtain the compositions of primary melts, we made inverse estimation by stepwise addition of equilibrated olivines from bulk-rock compositions until equilibrated olivines have Mg# = 90 to exclude the effect of fractional crystallization. The proportions of added olivine were calculated. With the assumption of complete incompatibility of H_2O in olivine in basaltic magmas, the H_2O contents in primary melts of Heishanling basalts were back calculated by adding the same amount of olivine to the magma diluting H_2O contents estimated by Cpx phenocrysts (Le Voyer et al., 2015). To diminish the interference by fractional crystallization, we applied the average magma H_2O contents calculated from early-crystallized Cpx phenocrysts with Mg# higher than 80 when back calculating the water contents in primary melts for individual samples by olivine addition. The water contents in primary melts have a range of 0.67-1.40 wt.% (Table S1) for individual Heishanling basalts, with the average of 1.03 ± 0.33 wt.%.

5. Discussion

5.1 Low degree of contamination by secondary processes

During their ascent to the surface, basaltic magmas may become chemically modified by contamination with crustal material around their flow channels or by later surficial alteration. The latter can notably increase the concentrations of LILE in basalts, but not those of HFSE. For all the basalts from the studied four localities (Heishanling, Chitucun, Leihuling and Yongxing) in Hainan Island, the observed good linear correlations between LILE (e.g., Rb, Ba; Figs. 9a-b) and Nb suggest that later alteration has not affected the compositions of these basalts. This is also supported by their low LOI values (<1 wt.%; Table S1; Gu et al., 2019). Contamination by crustal rocks can cause a significant increase in the $^{87}Sr/^{86}Sr$ ratios of the basalts along with their SiO_2 contents. This covariation has not been observed for any of the studied Hainan basalts (Fig. 9c), indicating no or only little contamination with crustal rocks. Furthermore, Ce/Pb and Nb/U in the Hainan basalts vary from 13.0 to 27.6 and from 27.9 to 49.0, respectively, with both ratios falling in or slightly below the range of global MORBs and OIBs (Hofmann et al., 1986), but being significantly higher than the corresponding ratios of the continental crust (Fig. 9d). No obvious correlation of $^{87}Sr/^{86}Sr$ or $^{143}Nd/^{144}Nd$ with Ce/Pb exists for Hainan basalts, even for the samples having Ce/Pb ratios lower than those of MORBs and OIBs (Figs. 9e and 8f). Additionally, crustal contamination may induce low εNd values, Nb/U ratios falling out of the global OIB range, and the positive correlation between εNd and MgO/SiO_2 ratios (Wang et al., 2013). However, these signatures do not occur to Heishanling samples (Figs. 9g and 9h). All these lines of evidence advocate that no significant crustal contamination has modified the compositions of our studied Hainan basalts.

5.2 Contribution of pyroxenite in the mantle source of Hainan basalts

Studies of natural samples and experimental investigations suggest that volatile-free peridotite cannot melt to generate magmas displaying the large variations in chemical and isotopic compositions or producing olivine phenocrysts with distinct compositions observed in many plume-related basalts (e.g., Dasgupta et al., 2007; Hauri, 1996; Herzberg, 2011; Pilet et al., 2008; Sobolev et al., 2005, 2007). Different models of the source lithological heterogeneity have been put forward to explain these observations, such as pyroxenite (e.g., Hauri, 1996; Herzberg, 2011; Sobolev et al., 2005, 2007), MORB-eclogite (no pyroxenite as an intermediate reaction product; e.g., Mallik and Dasgupta, 2012), carbonated peridotite (e.g., Dasgupta et al., 2007), or hornblendite (e.g., Pilet et al., 2008). Distinct geochemical or isotopic proxies have been proposed to indicate the contribution of pyroxenite in mantle sources (e.g., Herzberg, 2011; Le Roux et al., 2010; Sobolev et al., 2007). Pyroxenite in the upper mantle, where the dominate lithological constituent is peridotite, may be the product of reactions between subducted material with the ambient mantle in the solid state (Herzberg, 2011) or result from metasomatism of peridotite by partial melts from recycled material (Sobolev et al., 2007).

The compositions of bulk rocks and olivine phenocrysts from Hainan plume-related basalts suggest the presence of pyroxenite in their sources (An et al., 2017; Gu et al., 2019; Hoang et al., 2018; Liu J.Q. et al., 2015; Wang et al., 2012; Zhang et al., 2018b). For the Heishanling basalts, the high bulk-rock FeO/MnO and 1000*Zn/Fe ratios together with the relatively low CaO contents also require the presence of pyroxenite in their source (Fig. 10; Herzberg, 2011; Le Roux et al., 2010). All these observations mean that the Hainan plume has entrained a component related to subducted material, which are responsible for the generation of pyroxenite in the sources of the Cenozoic basalts occurring in southeastern Asia (Gu et al., 2019; Wang et al., 2012; Zhang et al., 2018b).

5.3 Compositional characteristics of the Hainan basalt source

The large compositional spectrum of mantle plume-related basalts has been ascribed to a large-scale heterogeneity in the mantle, which has been described using several endmembers compositions (Hofmann, 1997; White, 2015). The heterogeneity has been generally attributed to the contribution of recycled oceanic crust, continental upper or lower crusts, or sediments (Hofmann, 1997; Stracke et al., 2003; White, 2015; Willbold and Stracke, 2006). Several previous studies suggest that the basalts originally related to the Hainan mantle plume are partial melts of a mixture between EM II and the Pacific MORB source mantle (e.g., Flower et al., 1992; Tu et al., 1992; Yan et al., 2018; Zou and Fan, 2010). On the other hand, Tu et al. (1991) proposed that the source of the Hainan basalts may have been overprinted by subducted sediments.

Sr-Nd isotopic compositions of basalts from Heishanling and the other three localities display minor variations and fall in the range reported for enriched Cenozoic basalts from Hainan Island (Fig. 6). A conclusion similar to that of previous studies can be made that these samples originate from melting of an EM II-DMM mixture (Flower et al., 1992; Zou et al., 2010). $^{143}Nd/^{144}Nd$ of all our samples displays a negative correlation with Th/La, Rb/Nb and Ba/Nb but has a positive correlation with Nb/La (Figs. 11a, b, c, d). Several features in trace element compositions argue against direct contamination of Hainan basalts by material from the continental crust along their route to the surface: the lack of positive Pb anomalies; no negative Nb-Ta anomalies; and Ce/Pb and Nb/U ratios similar to those of global MORBs and OIBs; no correlation of $^{87}Sr/^{86}Sr$ ratios with SiO_2 contents and Ce/Pb ratios; no correlation of εNd values with MgO/SiO_2 and Nb/U ratios(Figs. 9c, d, e, g, h; Table S1). Mixing modeling (Langmuir et al., 1978) demonstrates that the source of the Hainan basalts is overprinted by recycled sedimentary material (Figs. 12a, b) and not solely recycled oceanic crust as proposed in previous studies (Liu J.Q. et al., 2015; Wang et al., 2013). Although the presence of subducted upper continental crustal rocks cannot be rejected in the source of the Hainan basalts, subducted sediments should be present to account for the high Ba/Th ratios in Hainan basalts (Fig. 12a; Plank and Langmuir, 1998). According to the quantitative model established by Stracke et al. (2003), the synthesized melt, which is produced by partial melting of the ambient mantle mixed with recycled oceanic crust and sediment, displays the trace element distribution pattern similar to those of Hainan basalts in this study (Fig. 13). This is consistent with the mixing modeling in Fig 12, both of which indicate that recycled sediment should have contributed to the mantle sources of

Hainan basalts.

5.4 Large range of H_2O/Ce ratios in Hainan basalts and its implications

As H_2O and Ce have a similar incompatibility during mantle melting, H_2O/Ce in basaltic magmas does not change during partial melting or later fractional crystallization and should thus closely approach the value of the mantle source (e.g., Bizimis and Peslier, 2015; Dixon et al., 2002). Because H_2O is much more mobile than Ce with released fluids during subduction and susceptible to diffusion during residence in the deep mantle, variable H_2O/Ce ratios can provide information on recycled material in basalt sources undergoing complex subduction processes. Based on the reverse calculation of water contents in magmas equilibrated with Cpx phenocrysts from Hainan basalts, H_2O/Ce ratios in the mantle source can be estimated to range from 50 to 425, i.e., extending from values previously reported for EM-type OIBs to values higher than those in MORBs (Table S1 and Gu et al., 2019). It is noteworthy that the magma water contents calculated by Gu et al. (2019) for the Chitucun, Leihuling and Yongxing basalts are well correlated with incompatible trace elements, such as Nb, La and Ce, which suggests that the recovered water contents were not affected by degassing or diffusion. The H_2O/Ce ratios of the Heishanling basalts from this study and the other Hainan basalts studied by Gu et al. (2019) show a negative correlation with $^{143}Nd/^{144}Nd$ (Fig. 14a; $R^2 = 0.5389$) and a positive one with $^{87}Sr/^{86}Sr$. In addition, the increase in H_2O/Ce also accompanies with the increase in $(Rb/Nb)_n$ (Fig. 14b) and $(Th/La)_n$ (Fig. 14c) in basalts. All these features mean that the “enriched” component in the mantle source has a high H_2O/Ce ratio. The observed high H_2O/Ce ratios (>420) in Hainan basalts are similar to those of the Cenozoic intraplate basalts in eastern China (Chen et al., 2017; Liu J. et al., 2015a, b; Xia et al., 2019) and the enriched MORBs in the Arctic ridge (Jan Mayen; Dixon et al., 2017), but rather distinct from the ratios in the EM I-and EM II-type OIBs, which show H_2O/Ce ratios of <100 (Dixon et al., 2002; Kendrick et al., 2014, 2015; Workman et al., 2006).

The enriched mantle endmembers components (HIMU, EM I, and EM II) have generally been related to diverse recycled material delivered by subducted slabs. All the surficial materials prior to subduction, such as altered oceanic crust and marine sediments, have very high H_2O/Ce ratios compared with the primitive mantle and DMM (Dixon et al., 2002; Shimizu et al., 2019). Even so, during subduction, selective loss of water can produce relative depletion of H_2O to Ce in residual slabs, which would be reflected in lower H_2O/Ce ratios in many OIBs that are geochemically more enriched by recycled material than NMORBs. The H_2O/Ce ratios of “enriched” mantle can vary from <80 to as high as ~425 (Fig. 1; Cabral et al., 2014; Dixon et al., 2017; Kendrick et al., 2014, 2015, 2017; Shimizu et al., 2019; Workman et al., 2006). The extremely low H_2O/Ce ratios have been explained by extreme dehydration of subducted slab components without later rehydration (Dixon et al., 2002, 2017; Kendrick et al., 2014, 2015) or water loss by diffusion during the residence of slabs in the lower mantle (Workman et al., 2006). In contrast, the high H_2O/Ce ratios of “enriched” mantle has been attributed to relatively hydrous components derived from subducted slabs at a shallower depth (above the mantle transition zone) with cool geothermal conditions (Dixon et al., 2017). For cooler slabs, materials at the upper part of slabs (e.g., sediments and altered oceanic crusts) could have experienced near-complete dehydration in shallow subduction zones, but at greater depths these ‘dry’ materials after dehydration could be rehydrated by fluids produced from subcrustal serpentinized oceanic lithospheric mantle (Dixon et al., 2017). This process induces the high H_2O/Ce ratios in the recycled sediments and altered oceanic crusts. This explanation is consistent with the observation that the OIB-like Cenozoic basalts in eastern China show high

H_2O/Ce ratios coupled with oxygen isotopic compositions ($\delta^{18}O$) distinct from that of the pristine mantle, which has been suggested to be a result of the release of hydrous components from the subducted Pacific slab stagnating in the mantle transition zone beneath eastern China (Chen et al., 2017; Liu J. et al., 2015a).

However, the scenario discussed above is not relevant in the Hainan case. Firstly, the study of basalts from the fossil spreading ridge in the South China Sea shows that the ambient asthenosphere did not contain hydrous components derived from a subducted slab at a shallow mantle, although there were multiple subduction events around the Hainan volcanic fields (Wang et al., 2019). Secondly, geophysical observations do not support the presence of any subducted slab segments in the mantle transition zone or upper mantle beneath Hainan island (Fukao et al., 2009; Li et al., 2008; Wei and Chen, 2016; Xia et al., 2016). This indicates that the high-H_2O/Ce components in the mantle sources of the Hainan basalts were derived from the deeper mantle and entrained by the Hainan mantle plume from the lower mantle. This is highly likely because mantle P wave topography imaging and plate reconstructions show that the Izanagi plate broke off and sank into the lower mantle before ~35 Ma, and the Hainan plume was triggered and entrained recycled material to generate the widespread Cenozoic basalts in the southeastern Asia (Kimura et al., 2018; Seton et al., 2015; Zhang and Li, 2018). According to the model of Dixon et al. (2017), the high H_2O/Ce ratio could be attributed to components derived from a less dehydrated part of the Izanagi plate segment, which would probably have a rather low geothermal gradient in the global subduction systems (Syracuse et al., 2010). While the low H_2O/Ce ratios (~50) could have resulted from extremely dehydrated oceanic basaltic rocks in an old subducted slab. As shown in Fig. 12, our modeling in the Ba/Th and Rb/Nb vs. $^{143}Nd/^{144}Nd$ diagrams supports this argument. Thus, the large variation in

H_2O/Ce compared to MORBs and the negative correlation of H_2O/Ce with $^{143}Nd/^{144}Nd$ in Hainan plume-related basalts suggest that recycled components incorporated into the Hainan plume entrained subducted plate material with different residence times in the lower mantle.

According to the batch melting model, the calculated water contents in the mantle source of the Heishanling basalts show a range from 279 to 582 ppm, assuming that the Heishanling basalts are products of a similar degree of partial melting to the Chitucun basalts, as based on their comparable trace element compositions (Gu et al., 2019). The estimated water contents in the source are considerably lower than the upper limit of the previously estimated values for global OIBs (300~1000 ppm; Hirschmann, 2006). Thus, although the H_2O/Ce ratio in the Hainan basalt source higher than DMM implies that recycled material entrained by the Hainan plume should have experienced relatively low degrees of dehydration, the source water content is generally lower than those in the mantle sources of LIPs. The observations of this study are still in favor of the conclusion made by Gu et al. (2019) that the low water content in the Hainan plume is likely the key factor that inhibited the generation of a LIP in response to the upwelling plume.

6. Concluding remarks

Cenozoic basalts dispersed in the northern part of Hainan Island have been originally related to the Hainan plume, the existence of which has been demonstrated by geophysical observations. The high FeO/MnO and 1000*Zn/Fe ratios and low CaO contents in bulk rocks suggest a contribution of pyroxenite, the generation of which has normally been related to the presence of subducted material in the mantle source of the Hainan basalts. Sr-Nd isotopic compositions, the covariation between $^{143}Nd/^{144}Nd$ and incompatible trace element ratios in bulk rocks, and the OIBtype trace element characteristics are consistent with a mantle source contaminated with recycled material, including subducted sediment and oceanic crust.

Water contents in the primary melt and mantle source of the Hainan basalts were retrieved from Cpx phenocryst compositions. H_2O/Ce in the mantle source ranges from 50 to 425, extending from values reported previously for EM-type OIBs to values higher than those of MORBs. Moreover, H_2O/Ce of the Hainan basalts covaries with $^{143}Nd/^{144}Nd$ and incompatible trace element ratios, indicating that higher H_2O/Ce ratios can be linked to recycled material in the source. These recycled components incorporated in the Hainan plume source may have undergone variable degrees of dehydration or deep rehydration by fluids released from subcrustal hydrous minerals during subduction.

Acknowledgements

This study was financially supported by the National Natural Science Foundation of China (grant nos. 41630205 and 41702046) and the Strategic Priority Research Program (B) of Chinese Academy of Sciences (grant no. XDB18000000). The two anonymous reviewers and the editor-in-Chief, Xian-Hua Li, are thanked for their constructive comments that have helped to largely improve the manuscript. We are grateful to Can Rao, Yan-Tao Hao and Su-Wen Qiu at the School of Earth Sciences, Zhejiang University (China), for their assistance with the analyses by EPMA and LA-ICPMS.

References

An, A.R., Choi, S.H., Yu, Y., Lee, D.C., 2017. Petrogenesis of Late Cenozoic basaltic rocks from southern Vietnam. Lithos 272-273, 192-204.

Bekaert, D.V., Turner, S.J., Broadley, M.W., Barnes, J.D., Halldórsson, S.A., Labidi, J., Wade, J., Walowski K.J., Barry, P. H., 2020. Subduction-Driven Volatile Recycling: A Global Mass Balance. Annual Review of Earth and Planetary Sciences 49, 37-70.

Bell, D.R., Ihinger, P.D., Rossman, G.R., 1995. Quantitative analysis of trace OH in garnet and pyroxenes. American Mineralogist 80, 465-474.

Bizimis, M., Peslier, A.H., 2015. Water in Hawaiian garnet pyroxenites: Implications for water heterogeneity in the mantle. Chemical Geology 397, 61-75.

Cabral, R.A., Jackson, M.G., Koga, K.T., Rosekoga, E.F., Hauri, E.H., Whitehouse, M.J., Price, A.A., Day, J.M.D., Shimizu, N., & Kelley, K.A., 2014. Volatile cycling of H_2O, CO_2, F, and Cl in the HIMU mantle: A new window provided by melt inclusions from oceanic hot spot lavas at Mangaia, Cook Islands. Geochemistry, Geophysics, Geosystems 15, 4445-4467.

Chen, H., Xia, Q.K., Ingrin, J., Deloule, E., Bi, Y., 2017. Heterogeneous source components of intraplate basalts from NE China induced by the ongoing Pacific slab subduction. Earth and Planetary Science Letters 459, 208-220.

Dasgupta, R., Hirschmann, M.M., Smith, N.D., 2007. Partial melting experiments of peridotite + CO_2 at 3 GPa and genesis of alkalic ocean island basalts. Journal of Petrology 48, 2093-2124.

Dixon, J.E., Clague, D.A., 2001. Volatiles in basaltic glasses from Loihi Seamount, Hawaii: Evidence for a relatively dry plume component. Journal of Petrology 42, 627-654.

Dixon, J.E., Leist, L., Langmuir, C., Schilling, J.G., 2002. Recycled dehydrated lithosphere observed in plume-influenced mid-ocean-ridge basalt. Nature 420, 385-389.

Dixon, J.E., Bindeman, I.N., Kingsley, R.H., Simons, K.K., Le Roux, P.J., Hajewski, T.R., Swart, P., Langmuir C.H., Ryan, J.G., Walowski, K.J., Wada, I., Wallace, P.J., 2017. Light stable isotopic compositions of enriched mantle sources: Resolving the dehydration paradox. Geochemistry, Geophysics, Geosystems 18, 3801-3839.

Ernst, R.E., Buchan, K.L., Campbell, I.H., 2005. Frontiers in large igneous province research. Lithos 79, 271-297.

Flower, M.F., Zhang, M., Chen, C.Y., Tu, K., Xie, G., 1992. Magmatism in the south China basin: 2. Post-spreading Quaternary basalts from Hainan Island, south China. Chemical Geology 97, 65-87.

Fukao, Y., Obayashi, M., Nakakuki, T., Deep Slab Project Group., 2009. Stagnant slab: a review. Annual Review of Earth and Planetary Sciences 37, 19-46.

Gale, A., Dalton, C.A., Langmuir, C.H., Su, Y., Schilling, J.G., 2013. The mean composition of ocean ridge basalts. Geochemistry, Geophysics, Geosystems 14, 489-518.

Gu, X.Y., Wang, P.Y., Kuritani, T., Hanski, E., Xia, Q.K., Wang, Q.Y., 2019. Low water content in the mantle source of the Hainan plume as a factor inhibiting the formation of a large igneous province. Earth and Planetary Science Letters 515, 221-230.

Hauri, E.H., 1996. Major-element variability in the Hawaiian mantle plume. Nature 382, 415-419.

Herzberg, C., 2011. Identification of source lithology in the Hawaiian and Canary Islands: Implications for origins. Journal of Petrology 52, 113-146.

Herzberg, C., Asimow, P.D., 2008. Petrology of some oceanic island basalts: PRIMELT2. XLS software for primary magma calculation. Geochemistry, Geophysics, Geosystems 9(9).

Hirschmann, M.M., 2006. Water, melting, and the deep Earth H_2O cycle. Annual Review of Earth and Planetary Sciences 34, 629-653.

Ho, K.S., Chen, J.C., Juang, W.S., 2000. Geochronology and geochemistry of late Cenozoic basalts from the Leiqiong area, southern China. Journal of Asian Earth Sciences 18, 307-324.

Hoang, N., Flower, M.F.J., Carlson, R.W., 1996. Major, trace element, and isotopic compositions of Vietnamese basalts: interaction of hydrous EM1-rich asthenosphere with thinned Eurasian lithosphere. Geochimica et Cosmochimica Acta 60, 4329-4351.

Hoang, T.H.A., Choi, S.H., Yu, Y., Pham, T.H., Nguyen, K.H., Ryu, J.S., 2018. Geochemical constraints on the spatial distribution of recycled oceanic crust in the mantle source of late Cenozoic basalts, Vietnam. Lithos 296-299, 382-395.

Hofmann, A.W., 1997. Mantle geochemistry: the message from oceanic volcanism. Nature 385, 219-229.

Hofmann, A.W., Jochum, K.P., Seufert, M., White, W.M., 1986. Nb and Pb in oceanic basalts: new constraints on mantle evolution. Earth and Planetary Science Letters 79, 33-45.

Jackson, M.G., Koga, K.T., Price, A., Konter, J.G., Koppers, A.A.P., Finlayson, V.A., Konrad, K., Hauri, E.H., Kylander-Clark, A., Kelley, K.A., Kendrick, M.A., 2015. Deeply dredged submarine HIMU glasses from the Tuvalu Islands, Polynesia: Implications for volatile budgets of recycled oceanic crust. Geochemistry, Geophysics, Geosystems 16, 3210-3234.

Kendrick, M.A., Jackson, M.G., Kent, A.J., Hauri, E.H., Wallace, P.J., Woodhead, J.D., 2014. Contrasting behaviours of CO_2, S, H_2O and halogens (F, Cl, Br, and I) in enriched-mantle melts from Pitcairn and Society seamounts. Chemical Geology 370, 69-81.

Kendrick, M.A., Jackson, M.G., Hauri, E.H., Phillips, D., 2015. The halogen (F, Cl, Br, I) and H_2O systematics of Samoan lavas: Assimilated-seawater, EM2 and high-$^3He/^4He$ components. Earth and Planetary Science Letters 410, 197-209.

Kendrick, M.A., Hemond, C., Kamenetsky, V.S., Danyushevsky, L.V., Devey, C.W., Rodemann, T., Jackson, M.G., Perfit, M.R., 2017. Seawater cycled throughout Earth's mantle in partially serpentinized lithosphere. Nature Geoscience 10, 222-228.

Kimura, J.I., Sakuyama, T., Miyazaki, T., Vaglarov, B.S., Fukao, Y., Stern, R.J., 2018. Plume-stagnant slab-lithosphere interactions: Origin of the late Cenozoic intra-plate basalts on the East Eurasia margin. Lithos 300-301, 227-249.

Kuritani, T., Nakagawa, M., Nishimoto, J., Yokoyama, T., Miyamoto, T., 2020. Magma plumbing system for the Millennium Eruption at Changbaishan volcano, China: Constraints from whole-rock U-Th disequilibrium. Lithos, 366-367, 105564.

Langmuir, C.H., Vocke Jr, R.D., Hanson, G.N., Hart, S.R., 1978. A general mixing equation with applications to Icelandic basalts. Earth and Planetary Science Letters 37, 380-392.

Le Roux, V., Lee, C.T. A., Turner, S.J., 2010. Zn/Fe systematics in mafic and ultramafic systems: Implications for detecting major element heterogeneities in the Earth's mantle. Geochimica et Cosmochimica Acta 74, 2779-2796.

Le Voyer, M., Cottrell, E., Kelley, K.A., Brounce, M., Hauri, E. H., 2015. The effect of primary versus secondary processes on the volatile content of MORB glasses: An example from the equatorial Mid-Atlantic Ridge, 5 °N-3 °S. Journal of Geophysical Research: Solid Earth 120, 125-144.

Li, C., Hilst, R.D.V.D., Engdahl, E.R., Burdick, S., 2008. A new global model for P wave speed variations in Earth's mantle. Geochemistry, Geophysics, Geosystems 9, Q05018.

Liu, J., Xia, Q.K., Deloule, E., Chen, H., Feng, M., 2015a. Recycled oceanic crust and marine sediment in the source of alkali basalts in Shandong, eastern China: Evidence from magma water content and oxygen isotopes. Journal of Geophysical Research: Solid Earth 120, 8281-8303.

Liu, J., Xia, Q.K., Deloule, E., Ingrin, J., Chen, H., Feng, M., 2015b. Water content and oxygen isotopic composition of alkali basalts from the Taihang Mountains, China: Recycled oceanic components in the mantle source. Journal of Petrology 56, 681-702.

Liu, J.Q., Ren, Z.Y., Nichols, A.R., Song, M.S., Qian, S.P., Zhang, Y., Zhao, P.P., 2015. Petrogenesis of Late Cenozoic basalts from North Hainan Island: Constraints from melt inclusions and their host olivines. Geochimica et Cosmochimica Acta 152, 89-121.

Makishima, A., Masuda, A., 1994. Ce isotope ratios of N-type MORB. Chemical Geology 118, 1-8.

Mallik, A., Dasgupta, R., 2012. Reaction between MORB-eclogite derived melts and fertile peridotite and generation of ocean island basalts. Earth and Planetary Science Letters 329-330, 97-108.

McDonough, W.F., Sun, S.S., 1995. The composition of the Earth. Chemical Geology 120, 223-253.

Montelli, R., Nolet, G., Dahlen, F., Masters, G., 2006. A catalogue of deep mantle plumes: New results from finite frequency tomography. Geochemistry, Geophysics, Geosystems 7 (11), Q11007.

Nichols, A. R. L., Carroll, M. R., Höskuldsson, Á., 2002. Is the Iceland hot spot also wet? Evidence from the water contents of undegassed submarine and subglacial pillow basalts. Earth and Planetary Science Letters 202, 77-87.

O'Leary, J.A., Gaetani, G.A., Hauri, E.H., 2010. The effect of tetrahedral Al^{3+} on the partitioning of water between clinopyroxene and silicate melt. Earth and Planetary Science Letters 297, 111-120.

Pilet, S., Baker, M.B., Stolper, E.M., 2008. Metasomatized lithosphere and the origin of alkaline lavas. Science 320, 916-919.

Pin, C., Briot, D., Bassin, C., Poitrasson, F., 1994. Concomitant separation of strontium and samarium-neodymium for isotopic analysis in silicate samples, based on specific extraction chromatography. Analytica Chimica Acta 298, 209-217.

Plank, T., Langmuir, C.H., 1998. The chemical composition of subducting sediment and its consequences for the crust and mantle. Chemical Geology 145, 325-394.

Richards, M.A., Duncan, R.A., Courtillot, V.E., 1989. Flood basalts and hot-spot tracks: plume heads and tails. Science 246, 103-107.

Rudnick, R.L., Gao, S., 2014. Composition of the continental crust, in: Rudnick, R.L. (Ed.), Treatise on Geochemistry, Second Edition. Elsevier, v. 4, pp. 1–51.

Seton, M., Flament, N., Whittaker, J., Müller, R.D., Gurnis, M., Bower, D.J., 2015. Ridge subduction sparked reorganization of the Pacific plate-mantle system 60-50 million years ago. Geophysical Research Letters 42, 1732-1740.

Shimizu, K., Ito, M., Chang, Q., Miyazaki, T., Ueki, K., Toyama, C., Senda, R., Vaglarov, B. S., Ishikawa, T., Kimura, J., 2019. Identifying volatile mantle trend with the water-fluorine-cerium systematics of basaltic glass. Chemical Geology 522, 283-294.

Sobolev, A.V., Hofmann, A.W., Sobolev, S.V., Nikogosian, I.K., 2005. An olivine-free mantle source of Hawaiian shield basalts. Nature 434, 590-597.

Sobolev, A.V., Hofmann, A.W., Kuzmin, D.V., Yaxley, G.M., Arndt, N.T., Chung, S.L., Danyushevsky, L.V., Elliott, T., Frey, F.A., Garcia, M.O., Gurenko, A.A., Kamenetsky, V.S., Kerr, A.C., Krivolutskaya, N.A., Matvienkov, V.V., Nikogosian, I.K., Rocholl, A., Sigurdsson, I.A., Sushchevskaya, N.M., Teklay, M., 2007. The amount of recycled crust in sources of mantle-derived melts. Science 316, 412-417.

Stracke, A., Bizimis, M., Salters, V.J., 2003. Recycling oceanic crust: Quantitative constraints. Geochemistry, Geophysics, Geosystems 4(3), 8003.

Sun, S.S., McDonough, W.F., 1989. Chemical and isotopic systematics of oceanic basalts: implications for mantle composition and processes. Geological Society, London, Special Publications 42, 313-345.

Syracuse, E.M., van Keken, P.E., Abers, G.A., 2010. The global range of subduction zone thermal models. Physics of the Earth and Planetary Interiors 183, 73-90.

Tian, Z.X., Yan, Y., Huang, C.Y., Dilek, Y., Yu, M.M., Liu, H.Q., Zhang, X.C., Zhang, Y., 2020. Fingerprinting subducted oceanic crust and Hainan Plume in the melt sources of Cenozoic Basalts from the South China Sea Region. Terra Nova 33, 21-29.

Tu, K., Flower, M.F., Carlson, R.W., Zhang, M., Xie, G., 1991. Sr, Nd, and Pb isotopic compositions of Hainan basalts (south China): implications for a subcontinental lithosphere Dupal source. Geology 19, 567-569.

Tu, K., Flower, M.F., Carlson, R.W., Xie, G., Chen, C.Y., Zhang, M., 1992. Magmatism in the South China Basin: 1. Isotopic and trace-element evidence for an endogenous Dupal mantle component. Chemical Geology 97, 47-63.

van Keken, P.E., Hacker, B.R., Syracuse, E.M., Abers, G.A., 2011. Subduction factory: 4. Depth-dependent flux of H_2O from subducting slabs worldwide. Journal of Geophysical Research: Solid Earth 116 (B1), B01401.

Walowski, K.J., Wallace, P.J., Hauri, E.H., Wada, I., Clynne, M.A., 2015. Slab melting beneath the Cascade Arc driven by dehydration of altered oceanic peridotite. Nature Geoscience 8, 404-408.

Wang, W., Chu, F., Wu, X., Li, Z., Chen, L., Li, X., Yan, Y., Zhang, J., 2019. Constraining Mantle Heterogeneity beneath the South China Sea: A New Perspective on Magma Water Content. Minerals 9(7), 410.

Wang, X.C., Li, Z.X., Li, X.H., Li, J., Liu, Y., Long, W.G., Zhou, J.B., Wang, F., 2012. Temperature, pressure, and composition of the mantle source region of Late Cenozoic basalts in Hainan Island, SE Asia: a consequence of a young thermal mantle plume close to subduction zones? Journal of Petrology 53, 177-233.

Wang, X.C., Li, Z.X., Li, X.H., Li, J., Xu, Y.G., Li, X.H., 2013. Identification of an ancient mantle reservoir and young recycled materials in the source region of a young mantle plume: implications for potential linkages between plume and plate tectonics. Earth and Planetary Science Letters 377-378, 248-259.

Wei, S.S., Chen, Y.J., 2016. Seismic evidence of the Hainan mantle plume by receiver function analysis in southern China. Geophysical Research Letters 43, 8978-8985.

White, W.M., 2015. Isotopes, DUPAL, LLSVPs, and Anekantavada. Chemical Geology 419, 10-28.

Willbold, M., Stracke, A., 2006. Trace element composition of mantle end-members: Implications for recycling of oceanic and upper and lower continental crust. Geochemistry, Geophysics, Geosystems 7(4), Q04004.

Workman, R.K., Hart, S.R., 2005. Major and trace element composition of the depleted MORB mantle (DMM). Earth and Planetary Science Letters 231, 53-72.

Workman, R.K., Hauri, E., Hart, S.R., Wang, J., Blusztajn, J., 2006. Volatile and trace elements in basaltic glasses from Samoa: Implications for water distribution in the mantle. Earth and Planetary Science Letters 241, 932-951.

Xia, Q.K., Liu, J., Liu, S.C., Kovács, I., Feng, M., Dang, L., 2013. High water content in Mesozoic primitive basalts of the North China Craton and implications on the destruction of cratonic mantle lithosphere. Earth and Planetary Science Letters 361, 85-97.

Xia, Q.K., Liu, J., Kovács, I., Hao, Y.T., Li, P., Yang, X.Z., Chen, H., & Sheng, Y.M., 2019. Water in the upper mantle and deep crust of eastern China: concentration, distribution and implications. National Science Review 6, 125-144.

Xia, S., Zhao, D., Sun, J., Huang, H., 2016. Teleseismic imaging of the mantle beneath southernmost China: New insights into the Hainan plume. Gondwana Research 36, 46-56.

Yan, Q., Shi, X., Castillo, P.R., 2014. The late Mesozoic-Cenozoic tectonic evolution of the South China Sea: a petrologic perspective. Journal of Asian Earth Sciences 85, 178-201.

Yan, Q., Shi, X., Metcalfe, I., Liu, S., Xu, T., Kornkanitnan, N., Zhang, H., 2018. Hainan mantle plume produced late Cenozoic basaltic rocks in Thailand, Southeast Asia. Scientific Reports 8, 2640.

Yu, M., Yan, Y., Huang, C.Y., Zhang, X., Tian, Z., Chen, W.H., Santosh, M., 2018. Opening of the South China Sea and upwelling of the Hainan plume. Geophysical Research Letters 45, 2600-2609.

Yu, X., Liu, Z., 2020. Non-mantle-plume process caused the initial spreading of the South China Sea. Scientific Reports 10, 8500.

Zhang, G.L., Luo, Q., Zhao, J., Jackson, M.G., Guo, L.S., Zhong, L.F., 2018a. Geochemical nature of sub-ridge mantle and opening dynamics of the South China Sea. Earth and Planetary Science Letters 489, 145-155.

Zhang, G.L., Sun, W.D., Seward, G., 2018b. Mantle source and magmatic evolution of the dying spreading ridge in the South China Sea. Geochemistry, Geophysics, Geosystems 19, 4385-4399.

Zhang, N., Li, Z.X., 2018. Formation of mantle “lone plumes” in the global downwelling zone-A multiscale modelling of subduction-controlled plume generation beneath the South China Sea. Tectonophysics 723, 1-13.

Zhao, D., Toyokuni, G., Kurata, K., 2021. Deep mantle structure and origin of Cenozoic intraplate volcanoes in Indochina, Hainan and South China Sea. Geophysical Journal International. 225, 572-588.

Zou, H., Fan, Q., 2010. U-Th isotopes in Hainan basalts: Implications for sub-asthenospheric origin of EM2 mantle endmember and the dynamics of melting beneath Hainan Island. Lithos 116, 145-152.

Fig. 1. H_2O/Ce vs. H_2O (in ppm) in mantle sources of OIBs representing compositionally different mantle endmembers. H_2O contents in sources were estimated according to the batch melting model from the retrieved H_2O contents of primary melts with partial melting degrees assigned to 5% for alkali OIBs and 10% for tholeiitic OIBs. Based on similar incompatibility of H_2O and Ce, H_2O/Ce ratios in melts is be assumed to represent those of their mantle sources. Data sources: PM, DMM and FOZO (Bizimis and Peslier 2015); EM I calculated from Pitcairn basalts (Kendrick et al., 2014); EM II calculated from Samoa (Kendrick et al., 2015) and Society basalts (Kendrick et al., 2014); HIMU calculated from Mangaia (Cabral et al., 2014) and Tuvalu basalts (Jackson et al., 2015); Hawaii basalt sources (Dixon and Clague, 2001; Shimizu, et al., 2019); Iceland basalt source (Nichols et al., 2002).

Fig. 2. (a) Distribution of Cenozoic basalts in southeastern Asia (modified after Yan et al., 2018)**.** The inserted small map shows the tectonic setting of southeastern Asia. Cenozoic basalts are dispersed over the Leiqiong area, the Beibu Gulf, the Indochina block and the South China Sea. The Leiqiong area refers to the Leizhou Peninsula and northern Hainan Island. **(b) Distribution of Cenozoic basalts with different eruption episodes in the northern part of Hainan Island and sample locations of this study.** Abbreviations: HSL = Heishanling, CTC = Chitucun, LHL = Leihuling (LHL), YX = Yongxing. The map is modified after Liu et al. (2015).

Fig. 3. Total alkali contents vs. SiO_2 contents for the Hainan basalts in this study. The grey dots represent Hainan basalts studied in Gu et al. (2019).

Fig. 4. Major and minor element variations in Hainan basalts. The arrows indicate effects of crystallization of different minerals (Ol = olivine, Cpx = clinopyroxene, Pl = plagioclase, Fe-Ti = Fe-Ti oxide). Data shown by gray symbols are from Gu et al. (2019).

Fig. 5. Chondrite-normalized rare earth element (REE) and primitive mantle-normalized trace element patterns for basalts from Hainan Island. Literature data on Leiqiong basalts (light blue field) taken from Liu et al.

(2015) and Wang et al. (2012) and Indochina basalts (grey field) from An et al. (2017), Hoang et al. (2018) and Yan et al. (2018). The data from Gu et al. (2019) are shown as grey lines. Normalization values taken from McDonough and Sun (1995). The reference compositions for OIB, continental crust (CC) and N-MORB are from Sun and McDonough (1989), Rudnick and Gao (2014) and Gale et al. (2013), respectively.

Fig. 6. ^{143}Nd/^{144}Nd vs. ^{87}Sr/^{86}Sr diagram for Hainan basalts. Reference data for MORBs, EM I-type OIBs (the Pitcairn and Tristan hotspots) and EM II-type OIBs (the Samoa, Society and Marquesas hotspots) were taken from the EarthChem database (www.earthchem.org). The data of Leiqiong basalts are from Tu et al. (1991), Wang et al. (2013) and Zou and Fan (2010) and the data of Indochina basalts from An et al. (2017), Hoang et al. (1996), Hoang et al. (2018) and Yan et al. (2018).

Fig. 7. Compositions of clinopyroxene phenocrysts from four samples of Heishanling basalt.

Fig. 8. Typical OH infrared absorption spectra for Cpx phenocrysts from Heishanling basalts. The dashed lines mark peak positions of individual OH bands at ~3640 cm^{-1}, ~3530 cm^{-1} and 3460 cm^{-1}. The absorbance has been normalized to a thickness of 1 cm.

Fig. 9. Plots of Rb vs. Nb (a), Ba vs. Nb (b), ^{87}Sr/^{86}Sr vs. SiO_2 (c), Ce/Pb vs. Nb/U (d), ^{87}Sr/^{86}Sr vs. Ce/Pb (e), ^{143}Nd/^{144}Nd vs. Ce/Pb (f), εNd vs. MgO/SiO_2 (g) and εNd vs. Nb/U (h) for Hainan basalts. In panels g and h, $\varepsilon Nd(t)=[(^{143}Nd/^{144}Nd)_{sample}/0.512638-1]\times10000$ (Wang et al., 2013). Chemical data from Chitucun, Leihuling and Yongxing (grey symbols) taken from Gu et al. (2019). The gray box in (d) represents the range of Nb/U and Ce/Pb ratios in global OIBs and MORBs (Hofmann et al., 1986). The Nb/U ratios of global OIBs and MORBs (grey zone) and continental crust (black line) are also from Hofmann et al. (1986). The composition of the continental crust is from Rudnick and Gao (2014).

Fig. 10. Variations of FeO/MnO (a), 10000*Zn/Fe (b) and CaO (c) as a function of MgO in bulk-rock

compositions of Hainan basalts. Literature data for Leiqiong basalts are from Flower et al. (1992), Ho et al. (2000), Liu et al. (2015), Wang et al. (2012) and Zou and Fan (2010) and those of Indochina basalts from An et al. (2017), Hoang et al. (1996), Hoang et al. (2018) and Yan et al. (2018). The range of FeO/MnO in peridotite melts in (a) is from Herzberg (2011) and the ranges of 1000*Zn/Fe in peridotite and pyroxenite melts in (b) from Le Roux et al. (2010). The green line separating pyroxenite and peridotite melts in (c) is from Herzberg and Asimow (2008).

Fig. 11. Relationship between $^{143}Nd/^{144}Nd$ and selected trace element ratios in Hainan basalts. Data from Gu et al. (2019) shown as grey symbols.

Fig. 12. Variation of Ba/Th and Rb/Nb with $^{143}Nd/^{144}Nd$ in Hainan basalts. Also shown are mixing lines calculated using the model of Stracke et al. (2003) and subducted sediments and oceanic crust with recycling ages of 2.0 and 2.5 Ga. The composition of DMM is from Workman and Hart (2005). Before subduction, sediments are thought to have compositions of GLOSS (Global Subducting Sediment; Plank and Langmuir, 1998). ROC refers to recycled oceanic crust, the individual ratios of which are calculated from Stracke et al. (2003). The black and green lines are calculated curves representing mixtures of DMM and subducted GLOSS and ROC with different subduction age of 2.0 Ga and 2.5 Ga, respectively (Langmuir et al., 1978). Data from Gu et al. (2019) plotted as grey symbols.

Fig. 13. Comparison of the trace element patterns of calculated melt and Hainan basalts. The composition of the calculated melt is derived from partial melting of the DMM+ROC mixture contaminated by 1.2 wt.% sediment. The quantitative model is according to the supplementary material named “TE_OIBmelts” from Stracke et al. (2003). The degree of melting is 4%, and assumes batch melting of eclogitic material. The composition of DMM, ROC and sediment are same with Fig. 12.

Fig. 14. Variation of H_2O/Ce with $^{143}Nd/^{144}Nd$ (a), $(Rb/Nb)_n$ (b) and $(Th/La)_n$ (c) in Hainan basalts. Data from Gu et al. (2019) plotted with grey symbols.

Table 1. Sr-Nd isotopic compositions of Hainan basalts measured in this study.

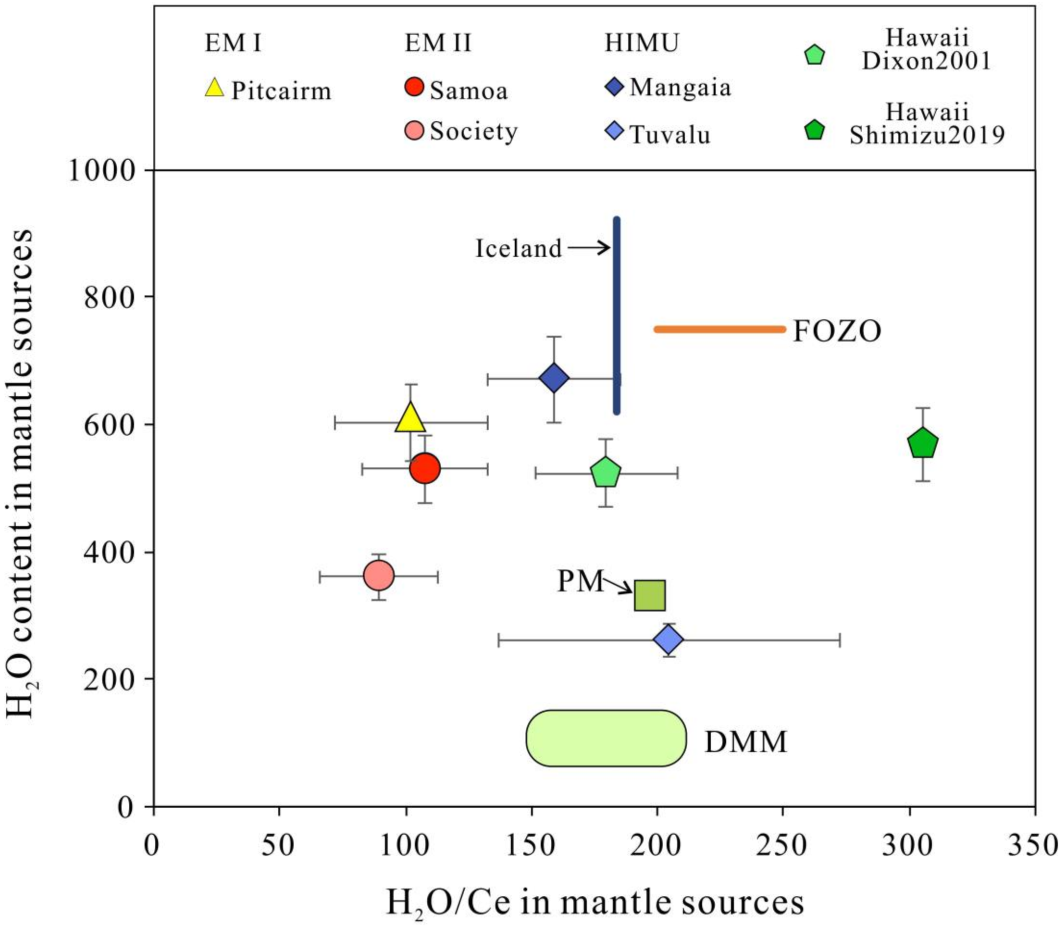
EM I
Pitcairm
EM II
Samoa
Society
HIMU
Mangaia
Tuvalu
Hawaii Dixon2001
Hawaii Shimizu2019
Iceland
FOZO
PM
DMM
H_2O content in mantle sources
H_2O/Ce in mantle sources
0
200
400
600
800
1000
0
50
100
150
200
250
300
350

Fig. 1

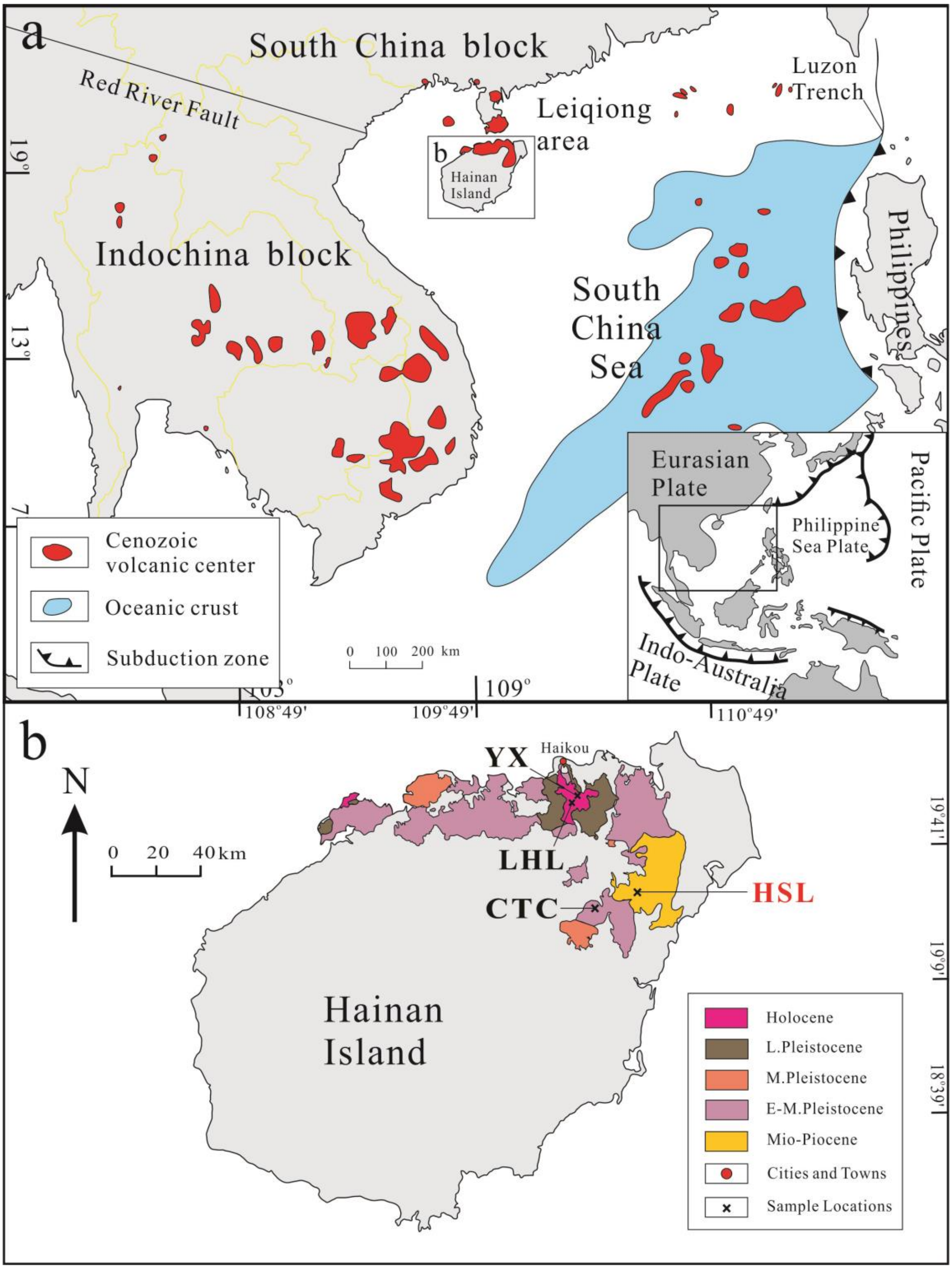
a
South China block
Red River Fault
Leiqiong area
Hainan Island
Luzon Trench
Indochina block
South China Sea
Philippines
Eurasian Plate
Pacific Plate
Philippine Sea Plate
Indo-Australia Plate
Cenozoic volcanic center
Oceanic crust
Subduction zone
0 100 200 km
19°
13°
7°
103°
109°
108°49'
109°49'
110°49'
b
N
0 20 40 km
YX
Haikou
LHL
CTC
HSL
Hainan Island
19°41'
19°9'
18°39'
Holocene
L.Pleistocene
M.Pleistocene
E-M.Pleistocene
Mio-Piocene
Cities and Towns
Sample Locations

652 **Fig. 2**

653

654 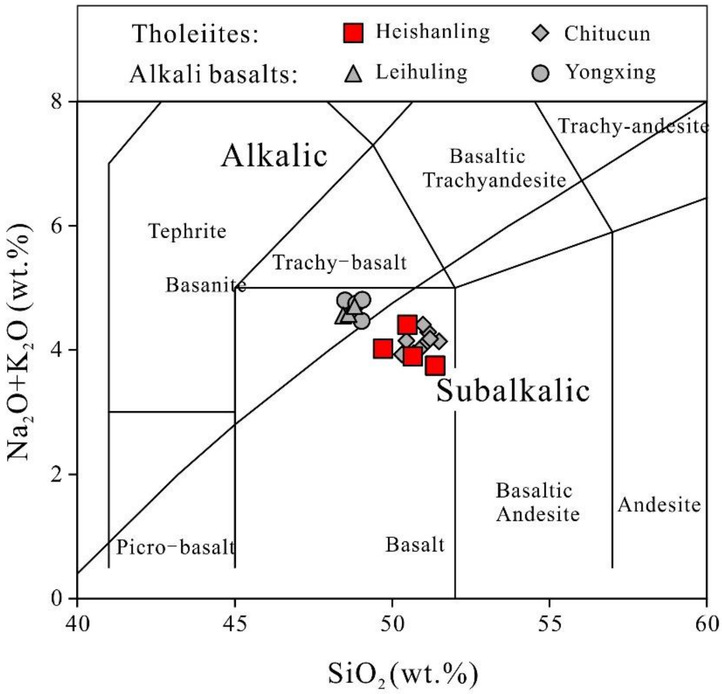

Tholeiites:
Heishanling
Chitucun
Alkali basalts:
Leihuling
Yongxing
Alkalic
Subalkalic
Tephrite
Basanite
Trachy-basalt
Basaltic Trachyandesite
Trachy-andesite
Picro-basalt
Basalt
Basaltic Andesite
Andesite
Na_2O+K_2O (wt.%)
SiO_2(wt.%)
0
2
4
6
8
40
45
50
55
60

655 **Fig. 3**

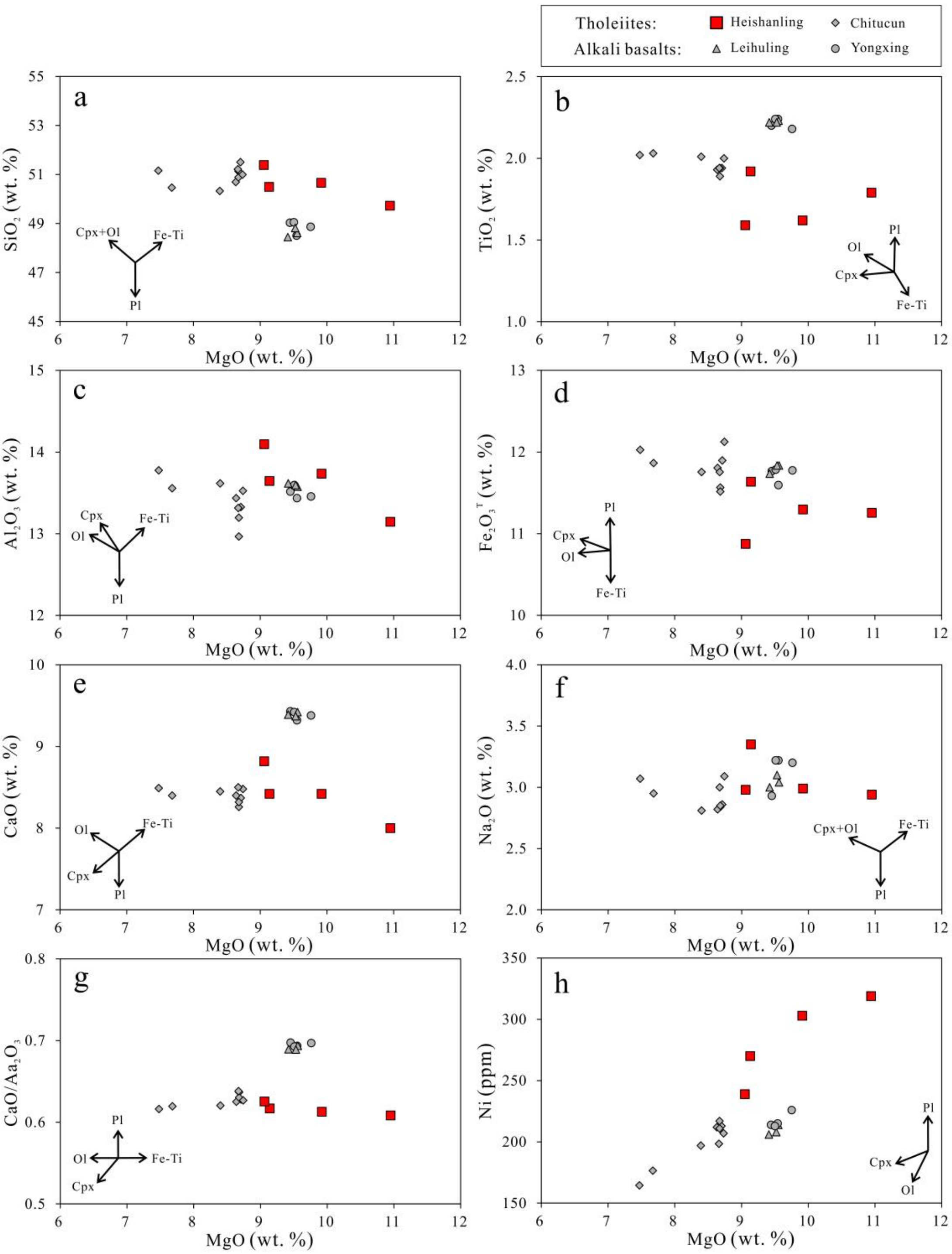
Tholeiites:
Heishanling
Chitucun
Alkali basalts:
Leihuling
Yongxing
a
b
c
d
e
f
g
h
SiO2 (wt. %)
TiO2 (wt. %)
Al2O3 (wt. %)
Fe2O3T (wt. %)
CaO (wt. %)
Na2O (wt. %)
CaO/Aa2O3
Ni (ppm)
MgO (wt. %)
Cpx+Ol
Fe-Ti
Pl
Ol
Cpx

Fig. 4

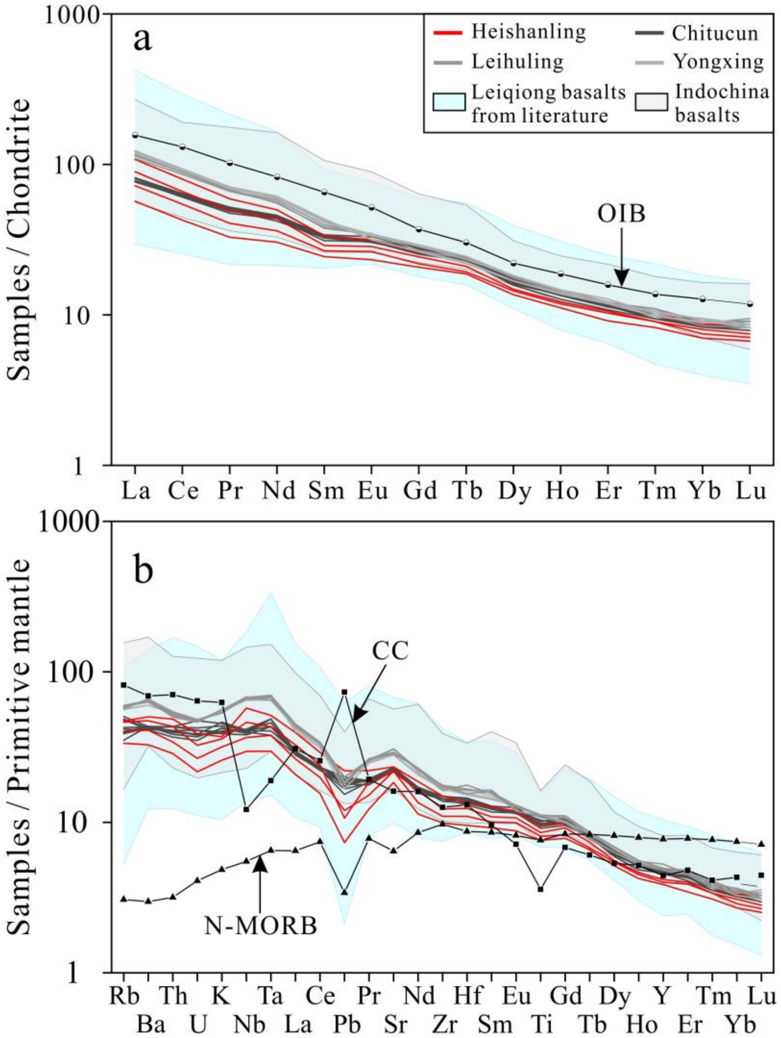
a
Heishanling
Chitucun
Leihuling
Yongxing
Leiqiong basalts from literature
Indochina basalts
OIB
Samples / Chondrite
1000
100
10
1
La Ce Pr Nd Sm Eu Gd Tb Dy Ho Er Tm Yb Lu
b
CC
N-MORB
Samples / Primitive mantle
1000
100
10
1
Rb Th K Ta Ce Pr Nd Hf Eu Gd Dy Y Tm Lu
Ba U Nb La Pb Sr Zr Sm Ti Tb Ho Er Yb

658 **Fig. 5**

659

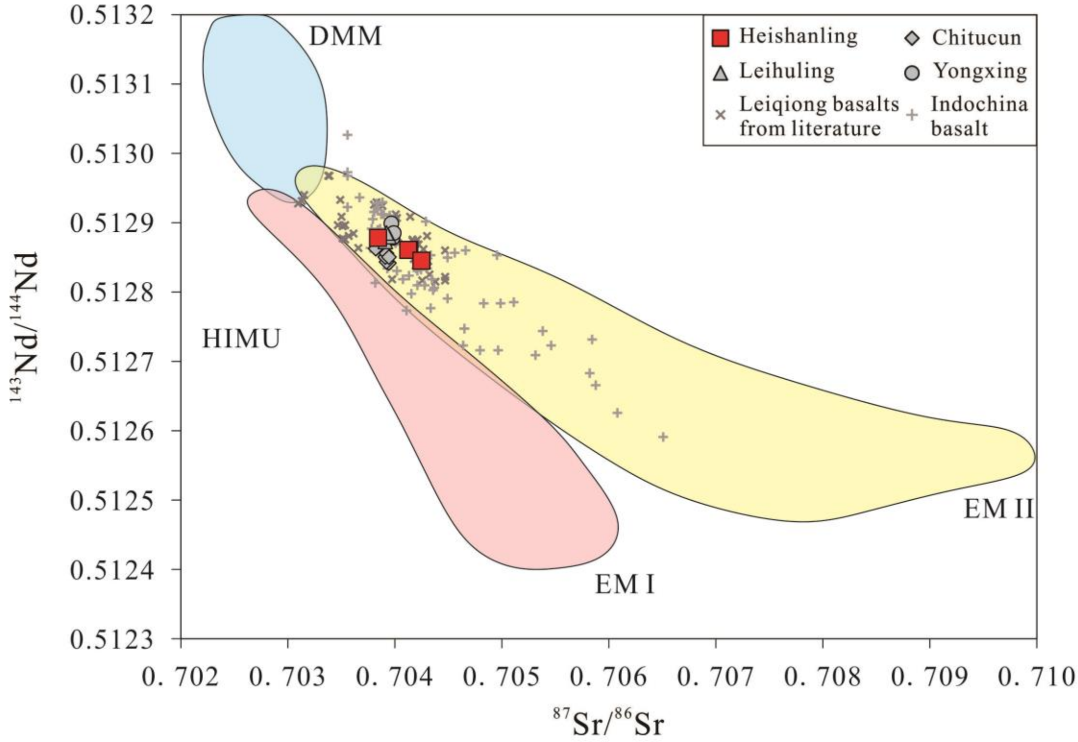

DMM
HIMU
EM I
EM II
Heishanling
Chitucun
Leihuling
Yongxing
Leiqiong basalts from literature
Indochina basalt
$^{143}Nd/^{144}Nd$
$^{87}Sr/^{86}Sr$
0.5132
0.5131
0.5130
0.5129
0.5128
0.5127
0.5126
0.5125
0.5124
0.5123
0. 702
0. 703
0. 704
0. 705
0. 706
0. 707
0. 708
0. 709
0. 710

660 **Fig. 6**

661

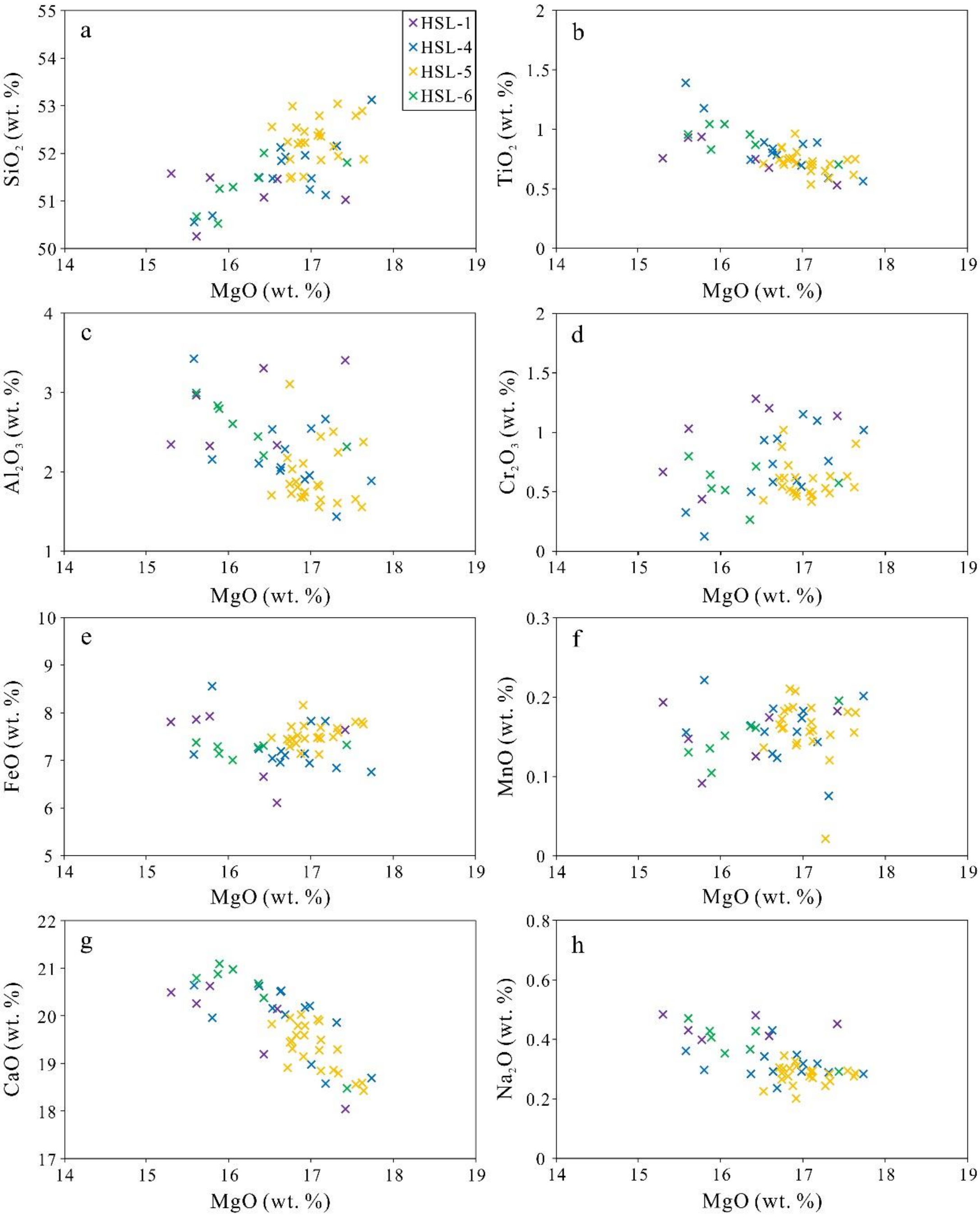
a
HSL-1
HSL-4
HSL-5
HSL-6
SiO_2 (wt. %)
MgO (wt. %)
b
TiO_2 (wt. %)
MgO (wt. %)
c
Al_2O_3 (wt. %)
MgO (wt. %)
d
Cr_2O_3 (wt. %)
MgO (wt. %)
e
FeO (wt. %)
MgO (wt. %)
f
MnO (wt. %)
MgO (wt. %)
g
CaO (wt. %)
MgO (wt. %)
h
Na_2O (wt. %)
MgO (wt. %)

Fig. 7

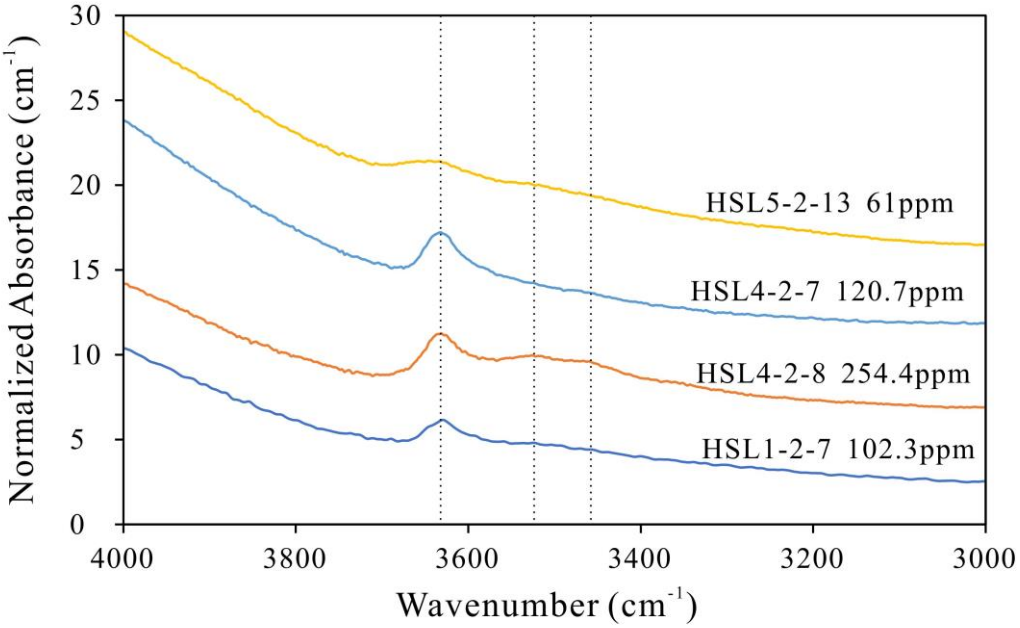
Normalized Absorbance (cm-1)
Wavenumber (cm-1)
HSL5-2-13 61ppm
HSL4-2-7 120.7ppm
HSL4-2-8 254.4ppm
HSL1-2-7 102.3ppm
30
25
20
15
10
5
0
4000
3800
3600
3400
3200
3000

Fig. 8

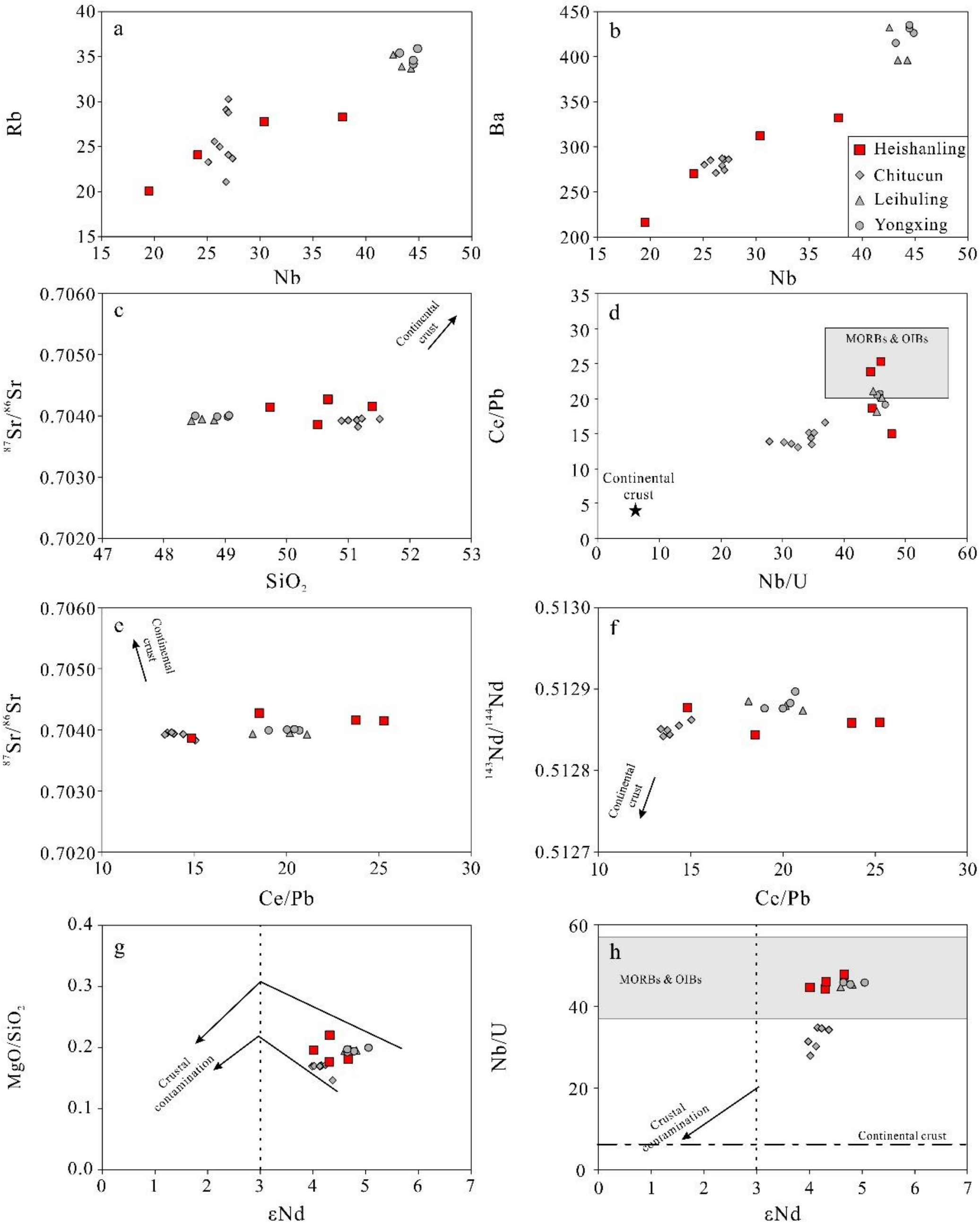
a
Rb
Nb
b
Ba
Nb
Heishanling
Chitucun
Leihuling
Yongxing
c
Continental crust
$^{87}Sr/^{86}Sr$
SiO_2
d
MORBs & OIBs
Continental crust
Ce/Pb
Nb/U
e
Continental crust
$^{87}Sr/^{86}Sr$
Ce/Pb
f
Continental crust
$^{143}Nd/^{144}Nd$
Ce/Pb
g
Crustal contamination
MgO/SiO_2
εNd
h
MORBs & OIBs
Crustal contamination
Continental crust
Nb/U
εNd

Fig. 9

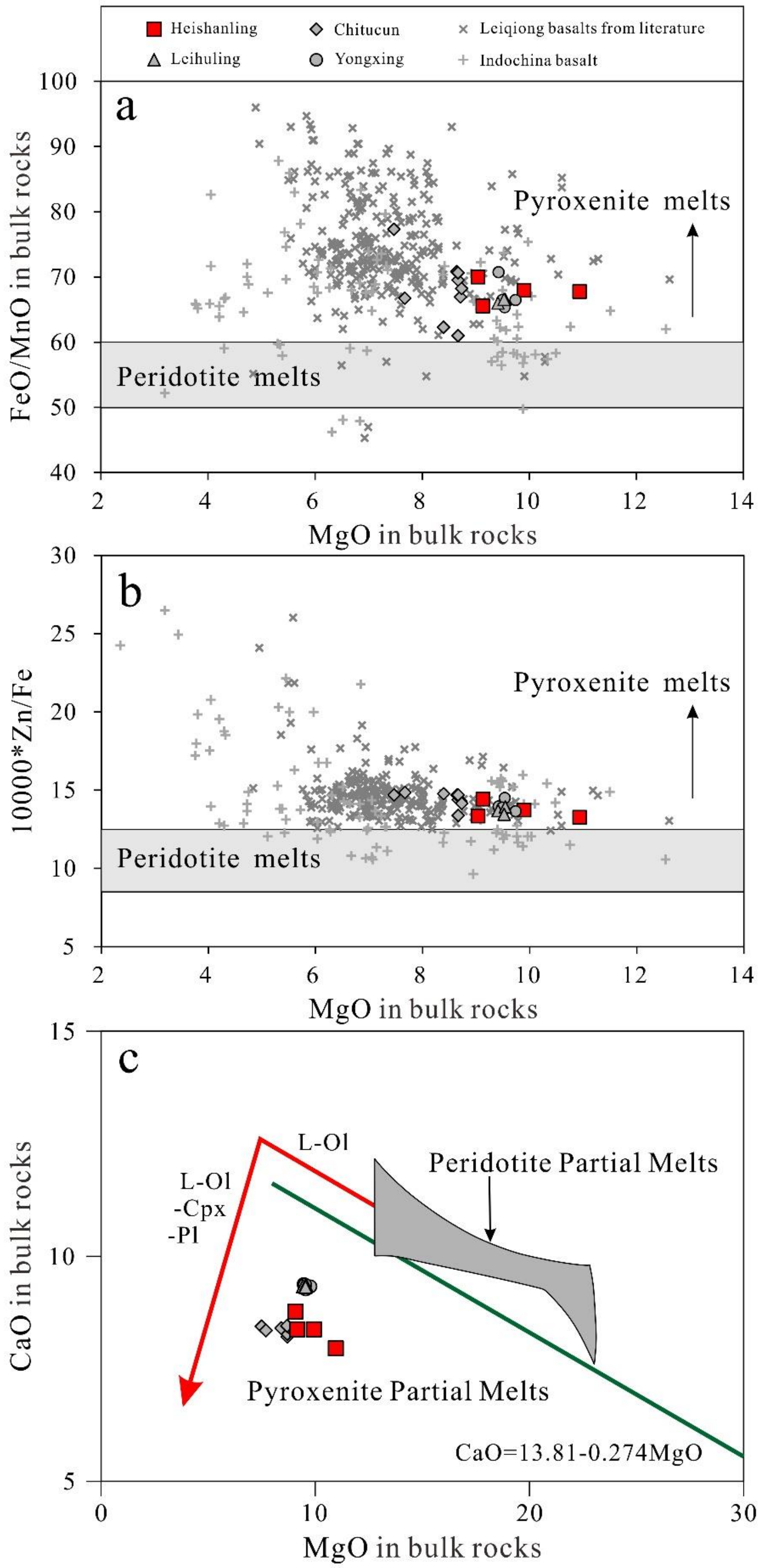

669 **Fig. 10**

670

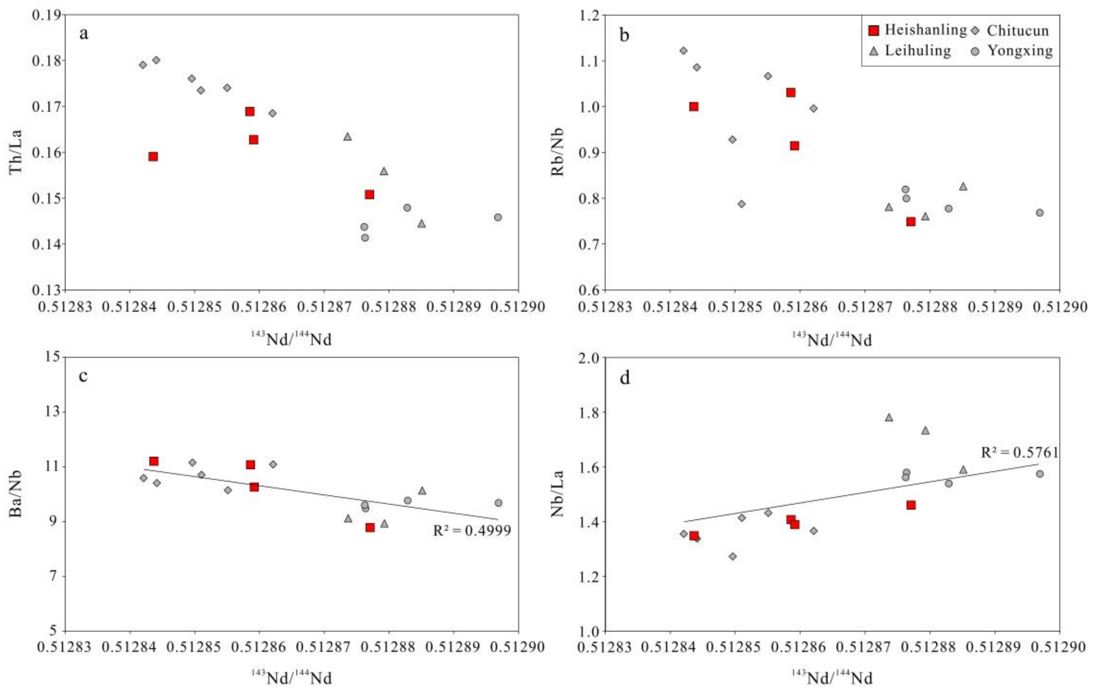

671 **Fig. 11**

672

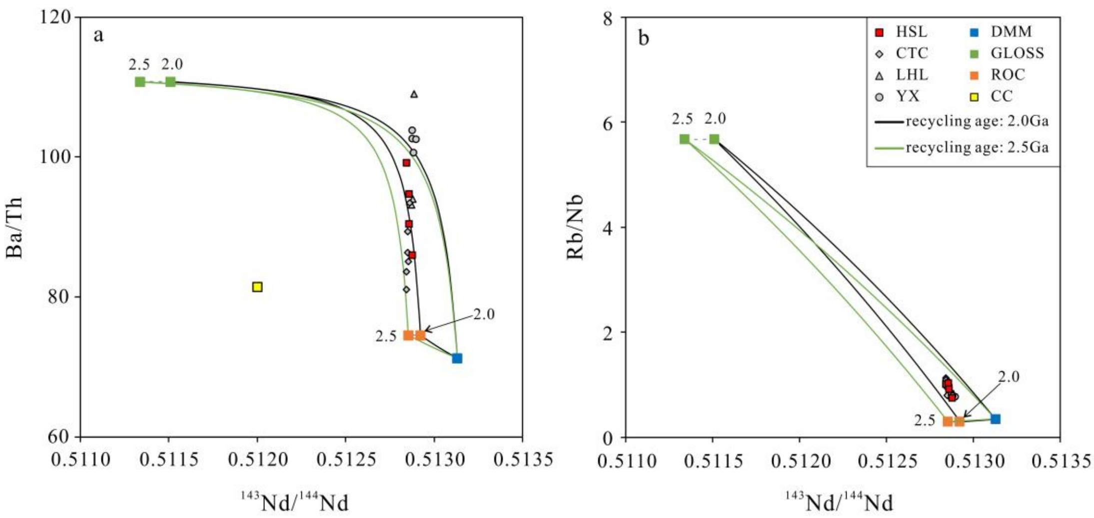

673 **Fig. 12**

674

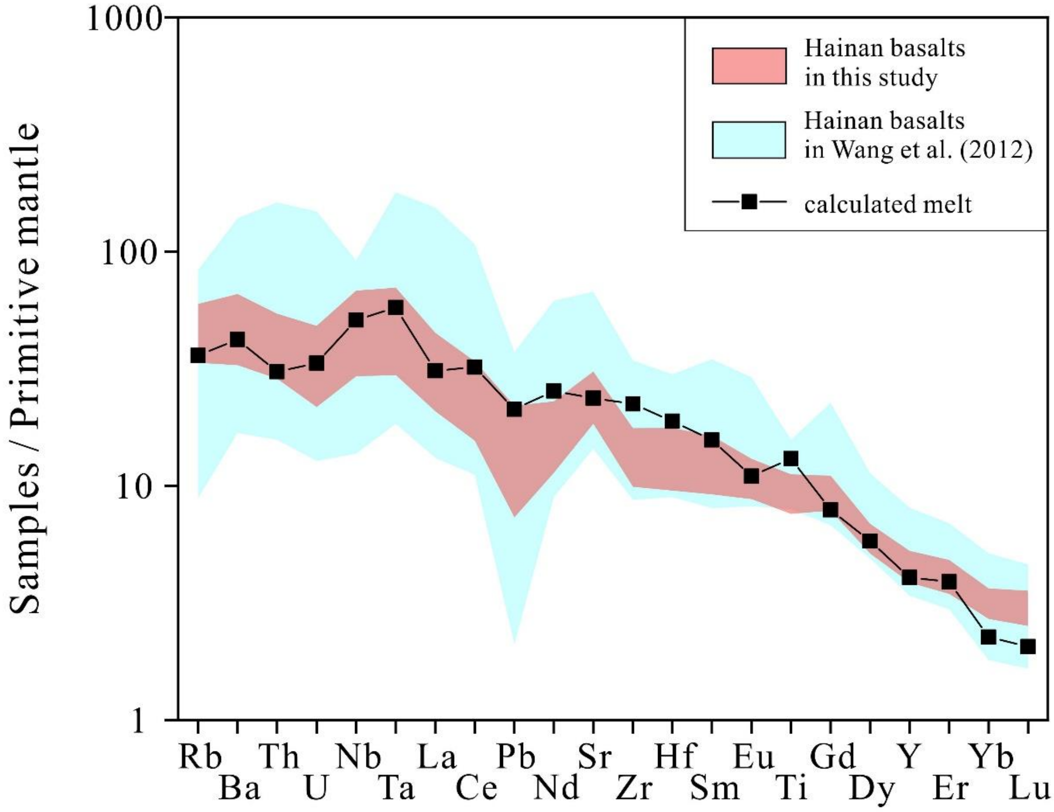

675

676 **Fig. 13**

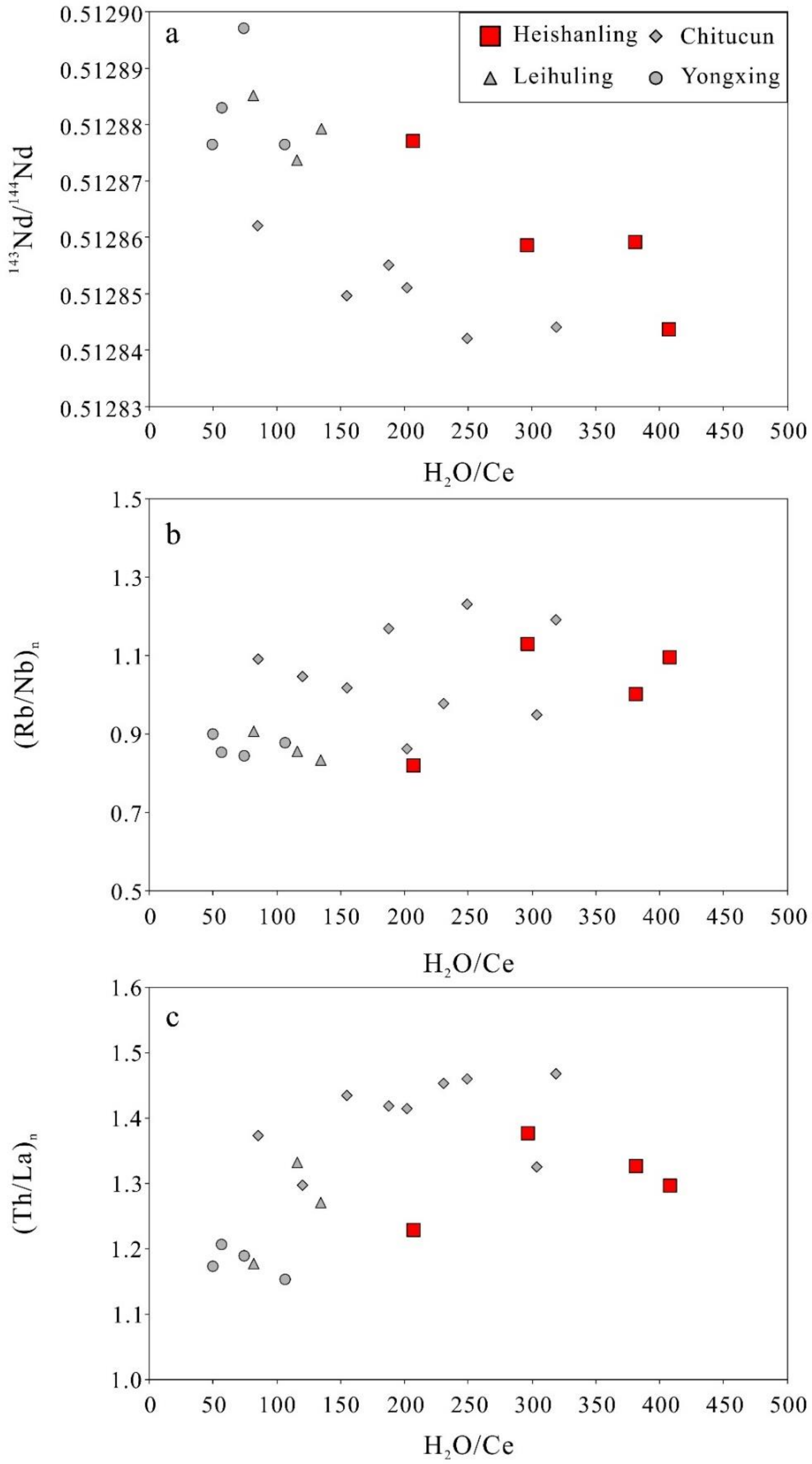

677

678 **Fig. 14**

679

Table 1. Sr-Nd isotopic compositions of Hainan basalts measured in this study.

Sample name	$^{87}Sr/^{86}Sr$	2se	$^{143}Nd/^{144}Nd$	2se
CTC1-1	0.703976	0.000008	0.512842	0.000007
CTC1-2	0.703960	0.000009	0.512844	0.000010
CTC1-4	0.703946	0.000010	0.512851	0.000011
CTC2-1	0.703849	0.000014	0.512862	0.000009
CTC2-4	0.703953	0.000013	0.512855	0.000009
CTC2-5	0.703982	0.000011	0.512850	0.000008
HSL-1	0.703885	0.000009	0.512877	0.000009
HSL-4	0.704296	0.000010	0.512844	0.000013
HSL-5	0.704180	0.000006	0.512859	0.000010
HSL-6	0.704169	0.000010	0.512859	0.000009
LHL-1	0.703946	0.000007	0.512874	0.000007
LHL-2	0.703973	0.000011	0.512879	0.000006
LHL-5	0.703954	0.000007	0.512885	0.000009
YX-1	0.704016	0.000009	0.512876	0.000007
YX-3	0.704028	0.000010	0.512876	0.000010
YX-4	0.704015	0.000012	0.512897	0.000011
YX-5	0.704034	0.000008	0.512883	0.000007